PAPER NO.

1653

STRESS WAVES IN SANDWICH PLATES

by

R. Kinslow, Tennessee Technological University

Presented at

1970 SESA FALL MEETING

Boston, Mass.

October 18-22

SOCIETY FOR
EXPERIMENTAL STRESS ANALYSIS
21 BRIDGE SQUARE WESTPORT, CONNECTICUT

SESA PAPER NO. 1653

STRESS WAVES IN SANDWICH PLATES*

by

Ray Kinslow**

TENNESSEE TECHNOLOGICAL UNIVERSITY

COOKEVILLE, TENNESSEE

OCTOBER, 1970

*This paper consists essentially of a portion of the report, "Stress Waves in Sandwich Plates," Report No. TTU-ES-70-3, prepared for the National Aeronautics and Space Administration, Manned Spacecraft Center, Houston, Texas, under Grant No. NGR-43-003-007, August, 1970.

**Professor and Chairman, Department of Engineering Science.

ABSTRACT

A mathematical stress wave model is formulated for use in predicting the effects of various material combinations and geometry in the design of sandwich plates that may be subjected to high velocity impact. In the experimental investigations the bounding layers were of a birefringent material and stresses were determined by means of a dynamic polariscope utilizing a high-speed framing camera. A comparison is made of the theoretical and experimental results.

CONTENTS

ILLUSTRATIONS

Figure

TABLES

NOMENCLATURE

c	wave velocity
E	Young's modulus
f	photoelastic constant
h	model thickness
k	constants
K	impedance mismatch
N	fringe order
0	point of impact
P_0	pressure at cavity surface
P	pulse amplitude
S	a point
r	radius vector
r_0	cavity radius
t	time
T	lamination thickness
u	particle displacement
v	particle velocity
y	distance from free surface of target
Y	target thickness
α	decay constant
ε_r	radial strain

ε_θ	tangential strain
λ, μ	Lamé constants
ν	Poisson's ratio
ϕ	scalar displacement potential
ρ	material density
σ_r	radial stress
σ_θ	tangential stress
τ	shear stress

SECTION I

INTRODUCTION

Meteoroids and other debris in outer space pose potential hazards to astronauts, spacecraft, and missiles. Although the impacted body may have sufficient strength and thickness to resist actual puncture, damage may be caused by strong shock waves resulting from the impact. When such a stress wave encounters a free surface, it is reflected, generally as a tensile wave. If the amplitude of this reflected wave is equal to or greater than the strength of the "target" material, fracture will occur. Such fractures may appear as cracks near the surface, weakening the structure; as rear surface bulges which could jam mechanisms or block flow in pipes; or as a complete detachment of target material, creating a shrapnel effect, endangering equipment or personnel.

It has been demonstrated that damage caused by stress waves produced by hypervelocity impact can, in many cases, be reduced by employing laminated targets (Reference 1). The results of such experiments have served to alert the design engineer to the possibility of reducing the probability of damage or of using a thinner or lighter material as the outer skin or hull of spacecraft. It is perhaps more important to realize that the use of laminates does not necessarily reduce the probability of damage, but may, in some cases, actually result in increased damage to the structure (Reference 2).

This study is an attempt to formulate a mathematical model that can be utilized to predict the action of laminates in affecting the stress waves induced by impact. Such a model should include all parameters that may affect the ability of structures to resist fracture caused by hypervelocity collisions before it can be used with confidence.

This study is limited to an investigation of elastic waves in sandwich plates or targets of only three layers, the two bounding layers being of one material and the center layer, or core, being of a different material. It deals only with stress amplitudes and not with material strengths and fracture criteria.

A brief theoretical analysis of the propagation of spherical stress waves is first made, followed by an experimental investigation of the stresses developed in both homogeneous and laminated targets.

A theoretical model is next formulated that duplicates the experimentally determined stresses in a homogeneous target as closely as possible. This is called a "quasi-theoretical" method (Reference 3). By using this theoretical model, the effects of the core are calculated and compared with those determined experimentally.

SECTION II

THEORETICAL ANALYSIS

Spherical dilatational wave propagation in homogeneous, isotropic material can be specified by the equation

$$\frac{\partial^2 \phi}{\partial t^2} = c^2 \left(\frac{\partial^2 \phi}{\partial r^2} + \frac{2}{r} \frac{\partial \phi}{\partial r} \right)$$

where ϕ is a scalar displacement potential, c is the wave velocity, and t is time. Particle displacement (u) and velocity (v) are specified by the relations

$$u = \frac{\partial \phi}{\partial r} \quad \text{and} \quad v = \frac{\partial u}{\partial t}$$

where r denotes the radius vector from the point of projectile impact. The radial and tangential stresses are given by the relations

$$\sigma_r = (\lambda + 2\mu)\left(\frac{\partial u}{\partial r}\right) + 2\lambda\left(\frac{u}{r}\right)$$

and

$$\sigma_\theta = \lambda \left(\frac{\partial u}{\partial r}\right) + 2(\lambda + \mu) \left(\frac{u}{r}\right)$$

where λ and μ are the Lamé constants and are related to Young's modulus (E)

and Poisson's ratio (ν) as follows

$$\lambda = \frac{E}{(1 + \nu)(1 - 2\nu)}$$

$$\mu = \frac{E}{2(1 + \nu)}$$

The mathematical model used in this investigation for generating spherical elastic waves is that described in References 4 and 5. It is assumed that there is a hollow hemispherical cavity in the target with its center at the point of impact and that a time-varying pressure or forcing function is applied to the cavity surface, generating stress waves in the target. The pressure (p_0) applied to the cavity surface is an impulse that may be described by the relation

$$p_0 = k_1 e^{-\alpha_1 t} + k_2 e^{-\alpha_2 t} + k_3 e^{-\alpha_3 t} + \cdots$$

where α_1, α_2, . . . are decay constants, t is elapsed time, and k_1, k_2, . . . are constants. By the proper choice of values of k and α, various wave forms can be generated.

The solution of the wave equation based upon Blake's work and described in Reference 5 is employed in this study.

The wave velocity is given by the relation

$$c = \left[\frac{E(1 - \nu)}{\rho(1 + \nu)(1 - 2\nu)} \right]^{1/2}$$

Figure 1 shows the target being considered. Its thickness is denoted by Y, and the distance of a point (S) from the origin (O) is denoted by r. Only stresses developed along the axis passing through O and normal to the target's rear surface have been considered.

Laminated Targets

An abrupt change in the physical properties of a material will result in the modification of a pressure pulse as it encounters this change. In general, a portion of the pulse will be transmitted, and a portion will be reflected. The relations which describe the modification of a pulse are based upon the boundary conditions of continuity of pressure and continuity of particle velocity across the interface between two materials. These relations depend upon the value of ρc, called the "characteristic impedance," of the two materials. If $\rho_0 c_0$ is for the first, and $\rho_t c_t$ is for the second laminate, and P_0 is the pulse amplitude in the first, the amplitude of the transmitted component is

$$P_t = \left[\frac{2\rho_t c_t}{\rho_t c_t + \rho_0 c_0} \right] P_0$$

and the reflected component is

$$P_r = \left[\frac{\rho_t c_t - \rho_0 c_0}{\rho_t c_t + \rho_0 c_0} \right] P_0$$

These relations are somewhat simplified by letting

$$K = \frac{\rho_t c_t}{\rho_0 c_0}$$

giving

$$P_t = \left[\frac{2K}{K + 1} \right] P_0$$

and

$$P_r = \left[\frac{K - 1}{K + 1} \right] P_0$$

The sandwich structure under consideration is shown in Figure 2. Its total thickness is Y, the thicknesses of the first and last layers of material are T_0 and T_2, respectively. The characteristic impedance of

both is $\rho_0 c_0$. The middle lamination has a thickness of T_1 and a characteristic impedance of $\rho_1 c_1$. This figure shows the distance-time relation of the wave fronts. Starting at time zero at point r_0, the wave moves with a velocity of c_0 through the first layer. Upon reaching the first interface, the amplitude of the transmitted component is $\left[\frac{2K}{K+1}\right] P_0$ which moves through the core at a velocity of c_1. As this pulse reaches the second interface, a portion will again be transmitted, and a part will be reflected. However, the value of the impedance mismatch at this interface is not K, but has a value of 1/K. The amplitude of the pulse transmitted is, therefore,

$$\left[\frac{2K}{K+1}\right]\left[\frac{2/K}{(1/K)+1}\right] P_0 = \left[\frac{2K}{K+1}\right]\left[\frac{2}{K+1}\right] P_0 = \left[\frac{4K}{(K+1)^2}\right] P_0$$

and is denoted by $P_{1\text{-}0\text{-}0}$. As only the stress developed in the last layer of the target is under consideration, it can be assumed that the target is composed of this material only, and that the initial pulse has an amplitude of $\left[\frac{4K}{(K+1)^2}\right] P_0$ instead of P_0. The time required, however, for this pulse to reach any point is not the same as for a homogeneous target due to the change in velocity through the core. It must be adjusted by the amount

$$t_{1\text{-}0\text{-}0} = \left[\frac{c_0 - c_1}{c_0 c_1}\right] T_1$$

The component of the pulse reflected from the second interface is $\left[\frac{K-1}{K+1}\right] P_0$, which, upon again reaching the first interface, will be reflected with an amplitude of $\left[\frac{K-1}{K+1}\right]^2 P_0$. A portion will then be transmitted through the second interface, this being

$$P_{2\text{-}0\text{-}0} = \left[\frac{K-1}{K+1}\right]^2 \left[\frac{4K}{(K+1)^2}\right] P_0 = \left[\frac{4K\,(1-K)^2}{(1+K)^4}\right] P_0$$

If the transmitted pulse amplitudes in this layer are denoted by P_{A-B-C}, the other pulses P_{A-0-0} may be specified as

$$P_{A-0-0} = \frac{4K(1 - K)^{2(A - 1)}}{(1 + K)^{2A}}$$

These pulse amplitudes, P_{1-0-0}, P_{2-0-0}, P_{3-0-0} . . . form a rapidly converging series, the sum of which approaches the value of P_0. This is to be expected, because pulse attenuation and energy losses have been neglected up to this time. The time adjustments for these waves are given by the relation

$$t_{A-0-0} = \frac{(2A - 1)c_0 - c_1}{c_0 c_1} T_1$$

Figure 3 gives the amplitudes of P_{A-0-0} as functions of the impedance mismatch, K.

Although the distance-time relations of all the wave fronts indicated by P_{A-B-C} are shown in Figure 2, only the amplitudes of P_{A-0-0} are considered in this paper as the other waves do not enter into the specific problem being investigated. Derivations of the other wave amplitudes and their contribution to the total stress in other targets are given in Reference 6. An analysis of stress waves in targets consisting of a large number of laminates may be found in Reference 7.

SECTION III

EXPERIMENTAL INVESTIGATION

In the experimental investigation described in this report, a Beckman and Whitley Model 201 synchronous framing camera was used to record the dynamic fringe pattern generated in the model. The camera is a rotating mirror type, making twelve 0.7 X 0.9-inch photographs on a 4 X 5-inch film at speeds up to one million frames per second. Exposure time for each photograph at this speed is approximately 0.6 microsecond. Figure 4 is a diagram of the camera and related equipment.

The two pulse generators deliver 100 Joules each at 5 KV. One was used to provide energy for the light source. After much experimentation with exploding wires and other devices, it was found that a Buss type AGC-1 safety fuse was an ideal light source. This fuse, when exploded, provides an intense light with a sufficiently long duration for satisfactory exposure of all twelve frames.

The other pulse generator was used as the energy source for generating stress waves in the model as a simulation of hypervelocity impact. After experimenting with many kinds of model materials, PSM-1, a clear polyester sheet manufactured by Photolastic, Inc., was selected as the basic material to be used in this study. Its manufacturer claims that it has the highest photoelastic sensitivity of any model material available and has a wave velocity of about 60,000 inches per second, sufficiently low to be photographed without apparent wave movement during exposure. Another important

factor is that it is practically free of creep and edge effects. This plastic can be easily machined, polished, and cemented to other materials. The most consistent stress waves were generated by exploding a fine wire in contact with one edge of the model. The amplitudes of these waves, however, were not sufficiently great for accurate comparison of waves having only slight differences in amplitude. A stronger shock, giving a greater number of fringes, resulted when a small amount of explosive was added. Urea nitrate was the explosive used in this investigation.

Separation of the stresses is possible without additional experimental data since the waves in this case propagate without rotation. Stresses are developed both along and perpendicular to the direction of wave propagation. Displacement occurs, however, only in the direction of wave motion. The displacements are specified by:

$$u_r = f(r) \quad , \quad u_\theta = 0$$

and the strain-displacement relations by

$$\varepsilon_r = \frac{du_r}{dr} \quad , \quad \varepsilon_\theta = \frac{u_r}{r}$$

The stress-strain equations are

$$\sigma_r = \frac{E}{1 - \nu^2} \left[\varepsilon_r + \nu\varepsilon_\theta\right] \quad , \quad \sigma_\theta = \frac{E}{1 - \nu^2} \left[\varepsilon_\theta + \nu\varepsilon_r\right]$$

and the shear stress has the value

$$\tau = \pm \frac{\sigma_\theta - \sigma_r}{2}$$

where E is Young's modulus and ν is Poisson's ratio.

From these relations

$$2\tau = \sigma_\theta - \sigma_r = \frac{E}{1 + \nu} \left[\varepsilon_\theta - \varepsilon_r\right] = \frac{E}{1 + \nu} \left[\frac{u_r}{r} - \frac{du_r}{dr}\right]$$

but

$$\frac{d}{dr}\left(\frac{u_r}{r}\right) = \frac{1}{r}\left[\frac{du_r}{dr} - \frac{u_r}{r}\right]$$

So

$$\sigma_\theta - \sigma_r = -\frac{E}{(1+\nu)}\left[r\frac{d}{dr}\left(\frac{u_r}{r}\right)\right]$$

$$\frac{d}{dr}\left(\frac{u_r}{r}\right) = -\frac{(1+\nu)}{E}\left(\frac{\sigma_\theta - \sigma_r}{r}\right)$$

$$\frac{u_r}{r} = -\frac{(1+\nu)}{E}\int\frac{\sigma_\theta - \sigma_r}{r}\,dr$$

$$\varepsilon_\theta = \frac{u_r}{r} = -\frac{2(1+\nu)}{E}\int\frac{\tau}{r}\,dr$$

$$\varepsilon_r = \varepsilon_\theta - \frac{2(1+\nu)}{E}\tau = -\frac{2(1+\nu)}{E}\left[\tau + \int\frac{\tau}{r}\,dr\right]$$

The radial and tangential stresses are, therefore,

$$\sigma_r = -\left(\frac{2}{1-\nu}\right)\left[\tau + (1+\nu)\int\frac{\tau}{r}\,dr\right]$$

$$\sigma_\theta = -\left(\frac{2}{1-\nu}\right)\left[\nu\tau + (1+\nu)\int\frac{\tau}{r}\,dr\right]$$

This derivation is essentially the same as that described in Reference 8. The stress-optic relation is

$$\tau = \frac{Nf}{2h}$$

where N is the fringe order, f is the photoelastic constant of the material, and h is the model thickness.

These relations may be stated in terms of the model material properties and the fringe order

$$u_r = -\frac{(1+\nu)f}{Eh}\left[r\int\frac{N}{r}\,dr\right] = r\varepsilon_\theta$$

$$\varepsilon_r = -\frac{(1+\nu)f}{Eh}\left[N + \int\frac{N}{r}\,dr\right] = \frac{du_r}{dr}$$

$$\varepsilon_\theta = -\frac{(1+\nu)f}{Eh}\left[\int\frac{N}{r}\,dr\right]$$

$$\sigma_r = -\frac{f}{h(1-\nu)}\left[N + (1+\nu)\int\frac{N}{r}\,dr\right]$$

$$\sigma_\theta = -\frac{f}{h(1-\nu)}\left[\nu N + (1+\nu)\int\frac{N}{r}\,dr\right]$$

Values of displacement, strain, and stress may now be determined by numerical integration.

As the objective of the present research is to compare the stresses developed in a laminated target with those produced in a homogeneous target under the same dynamic impulse, the properties of the material, such as the dynamic modulus of elasticity and photoelastic constant, have not been determined. Resulting strains, displacements, and stresses are, therefore, relative values only and are designated by $k_1\varepsilon$, $k_1 u$, and $k_2\sigma$ where $k_1 = E/f$ and $k_2 = 1/f$. Values of other properties for the target material, PSM-1, are: Poisson's ratio (ν) = 0.38, density (ρ) = 20 grams per cubic inch, thickness (h) = 0.25 inch, and wave velocity (c) = 60,500 inches per second. The characteristic impedance values of this and some other materials are given in Table I.

It was found that a light field polariscope utilizing circular polaroids, and a dark red filter gave the most satisfactory photographs

of the stress pattern. Figure 5 was prepared from three sets of photographs, shots 175, 176, and 177, and show fringe locations for each frame. Frame 12 of shot 175 was identical with frame 1 of shot 176, but there was a slight gap between the last frame of shot 176 and the first frame of shot 177. In the last frame of 176 the wave front is approaching the rear edge of the model and in 177 the wave is being reflected. The zero fringe (wave front) cannot be seen in these photographs because of the light field being used, so this fringe was determined by extrapolation from the other fringes. The broken line shows the approximate location of the reflected wave front.

Displacements, strains, and stresses were computed from values of r and N read from this figure. Figure 6 shows the photographs and computed results. Shots 175 and 176 were considered continuous with the frame numbers indicated as being from 1 to 23. Shot 177 was not included in the computations as this report does not deal with the waves reflected from a free surface.

A plot of fringe order versus distance for various times is shown in Figure 7. Computed displacements are shown in Figure 8; strains in Figure 9; and stresses in Figure 10. The different scales for the radial and tangential strain and stress should be noted.

Two targets were next prepared having cores of aluminum cemented to the PSM-1 with Eastman 910 epoxy. Referring to Table II, which gives impedance mismatch values for various combinations of materials, it is seen that the impedance mismatch between PSM-1 and aluminum is about nine.

In the first target, the core thickness was only 1/8 inch. Figure 11 shows ten frames of this shot (No. 240). The second target had a core

thickness of 1.0 inch. Figure 12 shows photographs of this shot (No. 226). Plots of the fringe order at a time of 68 microseconds and the computed stresses are shown in Figure 13. Only fringes 0.5 and 1.5 were developed in the latter, and as fringe number 1.5 was barely distinguishable, it was the maximum point on this curve.

The time of 68 microseconds corresponded to Frame 14 of the homogeneous target. A comparison of the stress waves in the homogeneous target and the two sandwich plates is made in Figure 14. The distances traveled are, of course, not the same, as the wave velocity in the aluminum was about four times as great as in the plastic.

SECTION IV

A QUASI-THEORETICAL SOLUTION

It was shown in Section II of this report that forcing functions can be selected that will closely simulate explosive impulses or hypervelocity impact. Therefore, it was desired to formulate a function that would approximately duplicate the experimentally determined pressure waves. Without going into the details of the procedure, it was found that the function

$$p_0 = 9{,}161\, e^{-0.01\,t} - 52{,}194\, e^{-0.02\,t} + 116{,}950\, e^{-0.03\,t} - 129{,}079\, e^{-0.04\,t} + 70{,}283\, e^{-0.05\,t} - 15{,}121\, e^{-0.06\,t}$$

shown in Figure 15 will, when multiplied by the proper constant and applied to a 2-inch spherical cavity, create a wave at a time of 68 microseconds that approximates the experimental wave as shown in Figure 16. The time of the theoretical wave has been adjusted by 32.6 microseconds, the time required for the wave to travel two inches, the assumed cavity radius. By employing a greater number of terms in the equation representing the forcing function, the theoretical wave could have been made to coincide with the experimental wave as closely as desired. Values of radial and tangential stresses at other times were computed and are shown in Figure 17. By comparing Figures 10 and 17 it is seen that the waves have the same amplitudes at a time of 68 microseconds but that the stress amplitudes do not attenuate at the

same rate. This is to be expected. The theoretical solution is for spherical waves which decay at a rate proportional to r^{-1}, but the experimental ones would be expected to be cylindrical waves in a thin plate. Theoretically, cylindrical waves attenuate at a rate proportional to $r^{-0.5}$. The expected attenuation of both spherical and cylindrical waves are compared with the experimental results in Figure 18. This shows that in reality, the experimental results are in closer agreement with the spherical than with the cylindrical wave attenuation.

Distance-time plots of the waves in the targets having 1/8- and 1.0-inch aluminum cores are given in Figure 19. It is seen that because of the geometry of the targets, only the waves P_{A-0-0} contribute to the stress in the third layer at the time under consideration.

The same forcing function applied to the homogeneous target was also applied to the sandwich plates. The radial stress-distance relations at the time of 68 microseconds were computed. The results are shown in Figure 20. This figure also shows each of the transmitted components, P_{A-0-0}, as well as their resultants. A comparison of these theoretical stresses in homogeneous and laminated targets is given in Figure 21.

SECTION V

CONCLUSION

The experimental and theoretical results given in Figures 14 and 21 are shown in Figure 22 with values normalized for comparison of maximum stresses. These may be summarized as follows:

	Maximum Stress Compared With Homogeneous Target	
	1/8" Core	1.0" Core
Experimental	0.72	0.41
Theoretical	0.86	0.42

There is practically no difference between the experimental and theoretical results in the case of the target with the one-inch core. In fact, one would expect the experimental error to be greater than the small difference that can be detected.

In the case of the 1/8-inch core, however, the agreement between theory and experiment is not as good. The experimental study indicated that the amplitude of the stress wave after passing through the core would be 72 percent of its amplitude in a homogeneous material. The theoretical analysis gives an amplitude of 86 percent.

There are several possible explanations of discrepancies between theoretical and experimental values. Some of these will be discussed briefly

so that they may be taken into consideration in future studies and may lead to more accurate and dependable results.

1. The experimental waves were generated and analyzed in 0.25-inch sheets, but the theoretical results were computed for spherical waves in semi-infinite targets. Close agreement would not be expected. Three-dimensional experiments employing an imbedded polariscope are being planned.
2. Explosives that generated the stress waves probably varied somewhat from shot to shot. More consistent results were obtained when wires were exploded without the use of chemical explosives. A more powerful energy source is needed so that a wire alone can be used and a greater number of fringes will be generated. Reference to Figure 13 will show that more fringes are needed to accurately define the amplitude of the stress wave that had passed through the 1/8-inch core. Although only the 0.5 and 1.5 fringes were created in the target having the 1.0-inch core, the peak of the wave was more accurately determined because the 1.5 fringe was barely visible in that frame.
3. It has been assumed that the cemented joints have no effect upon the transmitted and reflected waves. Two sheets of PSM-1 were cemented together and a stress wave photographed as it passed through the joint. No attenuation of the wave could be detected. As long as the effect

of the joint is small it will not materially affect the results in the case of a relatively thick core. With a one-inch laminate only two transmitted waves contributed to the maximum stress (Figure 20). The situation is much different when the core is thin. In the instance of the 1/8-inch core the resultant stress was dependent upon at least nine transmitted components. In this case there were ten waves transmitted through and sixteen reflections from the cemented joints. It is apparent that although an attenuation of stress may not be detected at a single joint it can be quite significant when there is a large number of reflections and transmissions. As previously stated, Eastman 910 cement was used in the construction of the models used in this study. More attention should probably be given to selecting a cement having a characteristic impedance equal to that of the model material. Any voids in the cemented joint will, of course, have a large effect on the experimental results.

4. It has been assumed that the wave velocity remains constant in any given material. Only the first component (P_{1-0-0}) passes through undisturbed material. The reflected waves may traverse the core material many times. The material density and elastic constants will probably be changed slightly, perhaps due

to heating of the material. This will cause some change in the wave velocity and in the characteristic impedance (ρc) of the material. (It has been shown that the velocity of a reflected wave in Lucite is about 80 percent of that of the incident wave [Reference 2]).

5. Energy losses have been neglected. This is obviously not a valid assumption although these losses may be small.

As it is impossible to experimentally test even a small percentage of all possible material combinations of which sandwich plates may be constructed, a dependable theoretical method of analysis is needed. It is believed that the semi-empirical method developed in this study may be used to predict the effects of various material combinations and be of value in the design of sandwich plates that may be subjected to high velocity impact. It is shown that the multiple reflections within the structure must be taken into consideration.

REFERENCES

1. Kinslow, Ray, "Stress Waves in Composite Laminates," AEDC-TR-65-69, June, 1965.

2. Kinslow, Ray, "Observations of Hypervelocity Impact of Transparent Plastic Targets," AEDC-TDR-64-49 (AD438947), May, 1964.

3. Cosby, William A., and Lyle, Robert G., "The Meteoroid Environment and Its Effects on Materials and Equipment," NASA SP-78, 1965.

4. Kinslow, Ray, "Properties of Reflected Stress Waves," AEDC-TR-67-112 (AD818630), August, 1967.

5. Kinslow, Ray, "Properties of Spherical Stress Waves Produced by Hypervelocity Impact," AEDC-TDR-63-197 (AD421578), October, 1963.

6. Kinslow, Ray and Delano, Brian, "Stress Waves in Sandwich Plates," TTU-ES-70-3, August, 1970.

7. Kinslow, Ray, "Stress Waves in Multiple Laminates," TTU-ES-70-1, NASA CR-89880, March, 1970.

8. Dally, J. W. and Riley, W. F., "Stress Wave Propagation in a Half-Plane Due to Transient Point Load," Developments in Theoretical and Applied Mechanics, ed. by W. A. Shaw, Vol. 3, Pergamon Press, London, 1967, pp. 357-377.

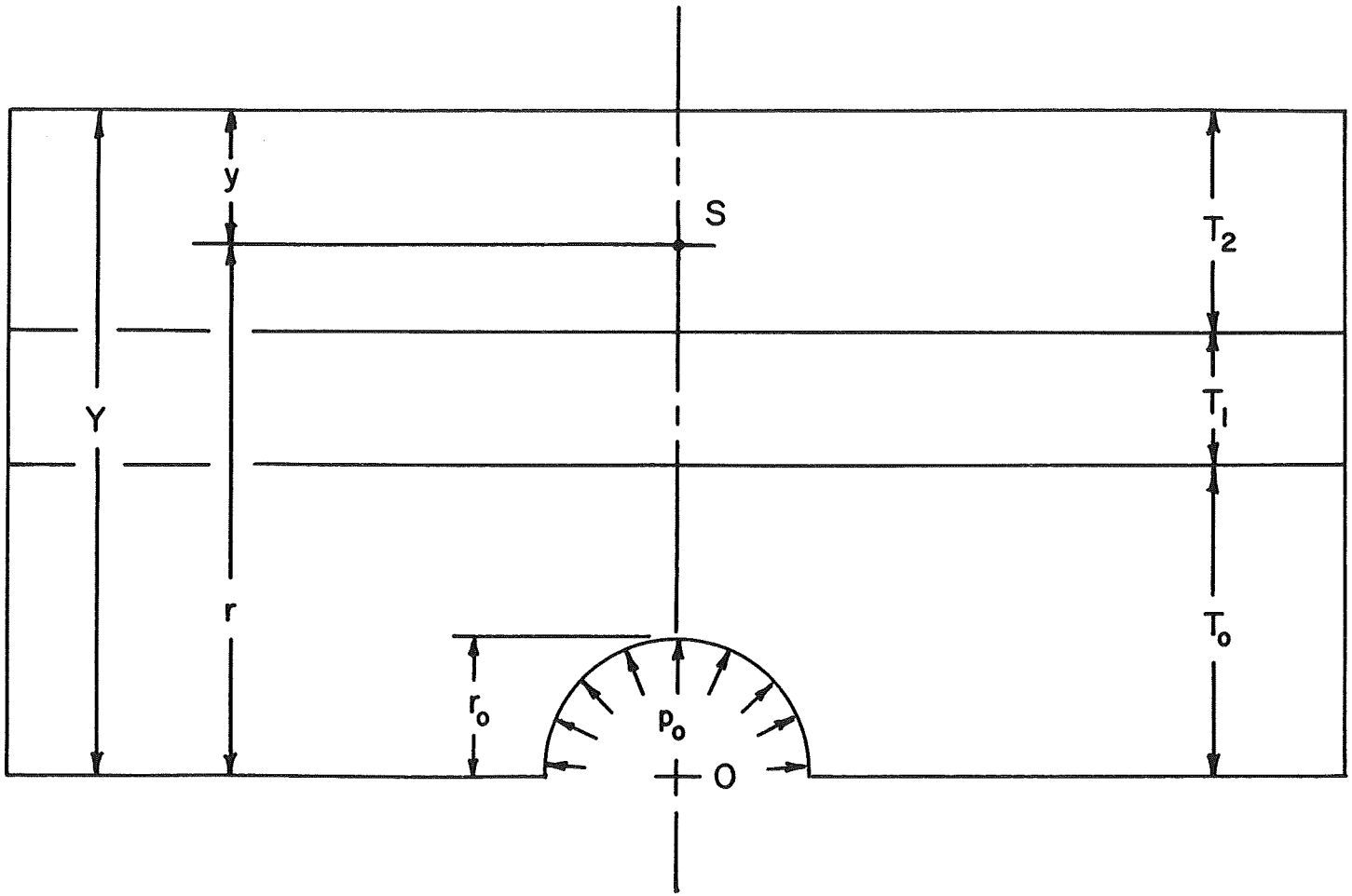

FIGURE 1

TARGET DIMENSIONS AND COORDINATES

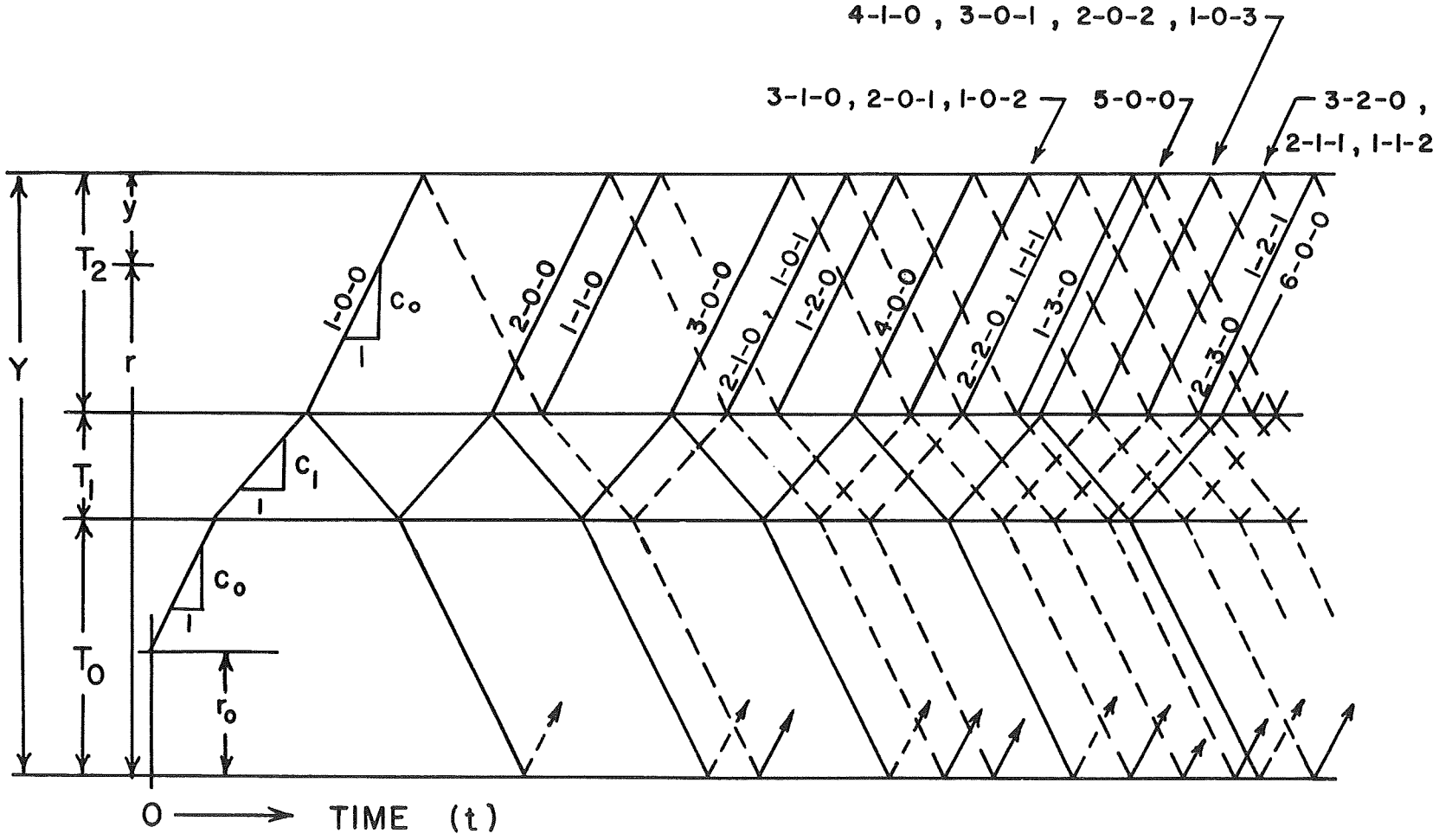

FIGURE 2

REFLECTED AND TRANSMITTED STRESS WAVES IN LAMINATED TARGETS

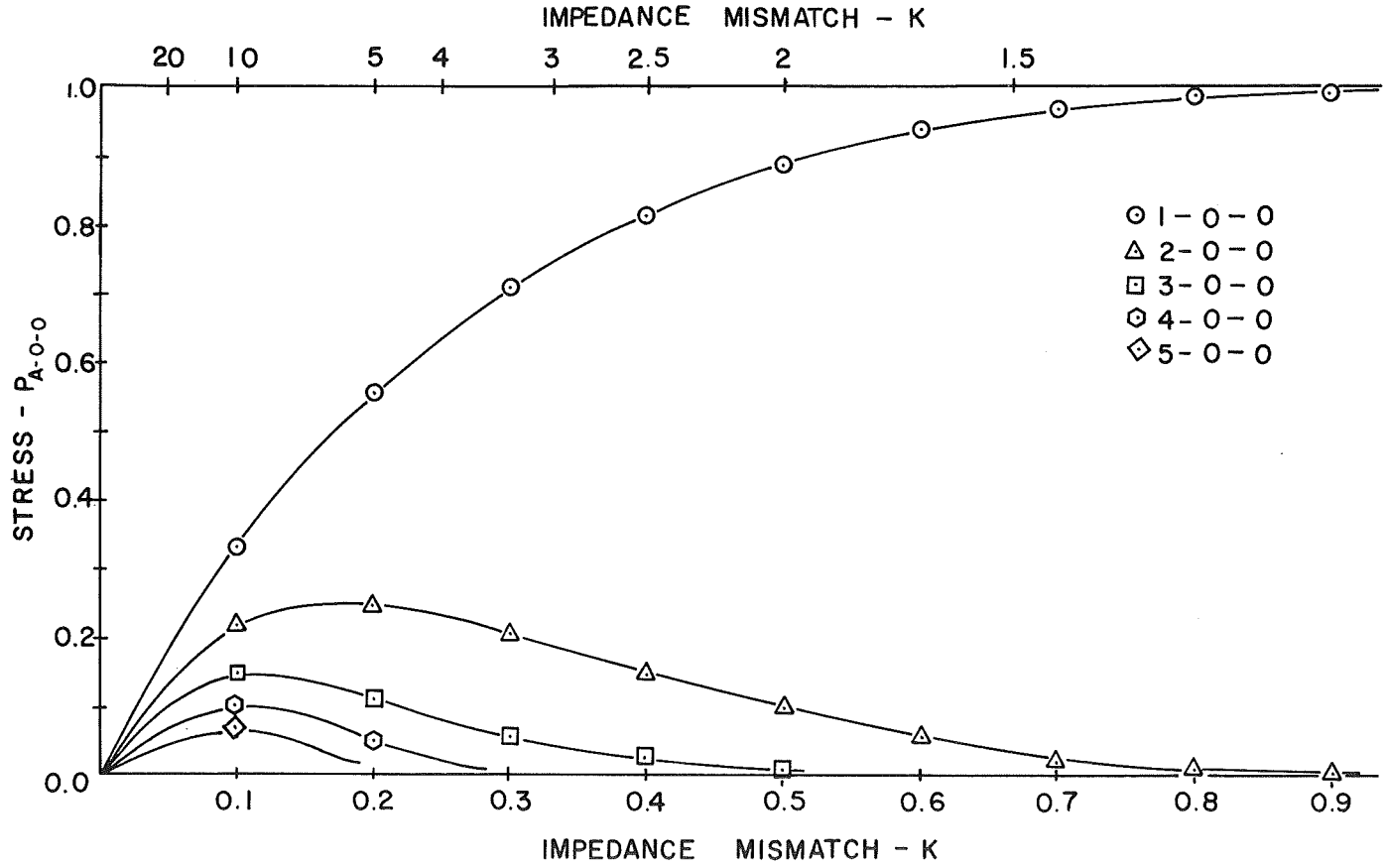

FIGURE 3

STRESS AMPLITUDE - IMPEDANCE MISMATCH RELATIONS

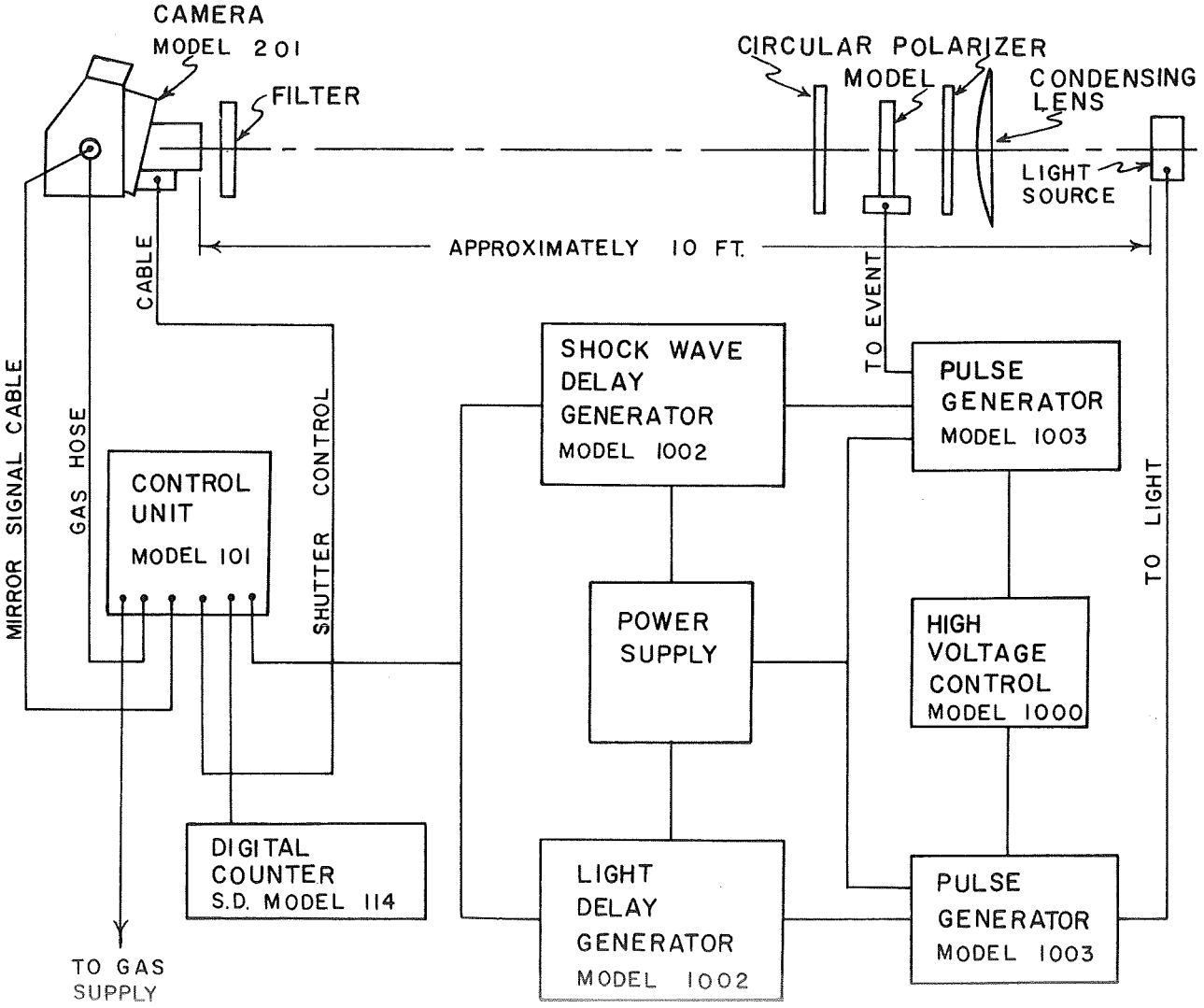

FIGURE 4

POLARISCOPE, CAMERA, AND CONTROLS

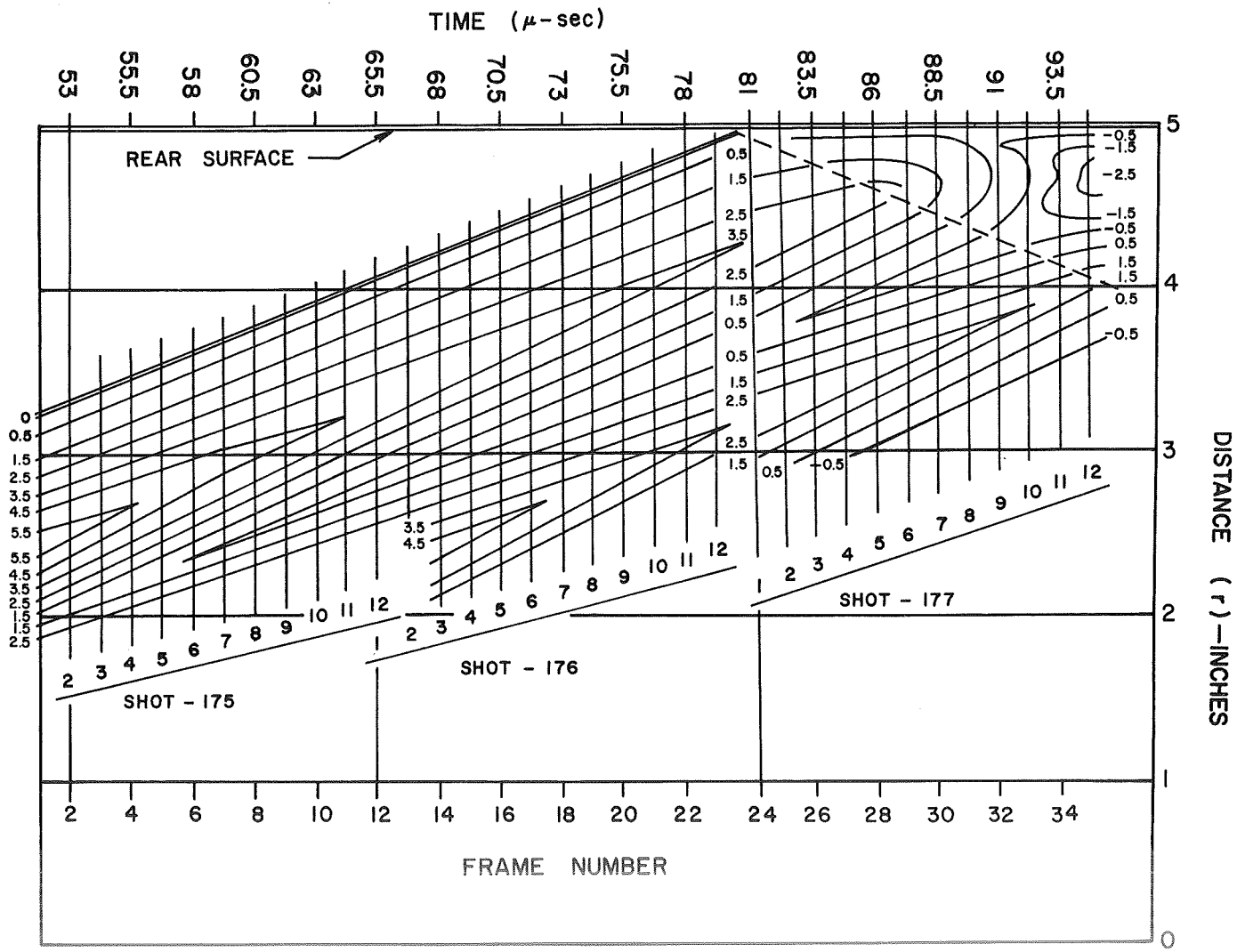

FIGURE 5

FRINGE LOCATIONS AT VARIOUS TIMES

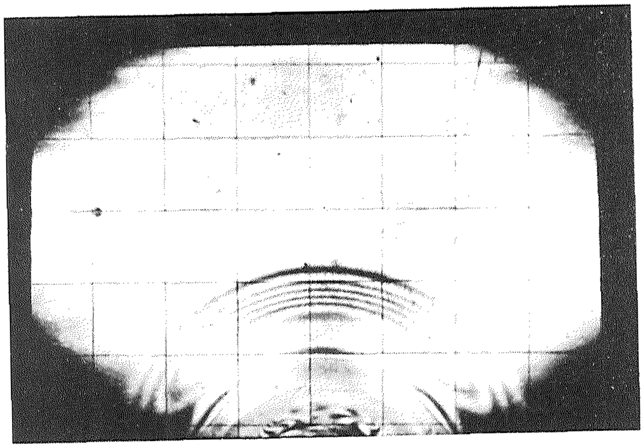

SHOT NUMBER 175, FRAME NUMBER 2

	N	R	UR	ET	ER	SIGMA R	SIGMA THETA
1	0.0	3.290	0.0	0.0	0.0	0.0	0.0
2	0.500	3.200	0.124	0.039	-2.721	-3.163	-1.163
3	1.500	3.050	0.937	0.367	-7.773	-9.182	-3.182
4	2.500	2.940	2.131	0.715	-13.045	-14.976	-4.976
5	3.500	2.830	3.810	1.348	-17.372	-20.406	-6.406
6	4.500	2.720	6.002	2.226	-22.614	-25.442	-7.442
7	5.500	2.580	9.516	3.549	-26.671	-29.534	-7.534
8	5.500	2.480	12.226	4.427	-25.433	-27.537	-5.537
9	4.500	2.380	14.626	5.061	-16.779	-17.256	-1.256
10	3.500	2.280	15.975	7.007	-12.313	-11.290	2.720
11	2.500	2.200	16.712	7.537	-6.203	-3.877	6.123
12	1.500	2.130	16.935	7.752	-0.328	3.149	9.149
13	1.200	2.070	16.931	8.165	1.941	5.427	10.227
14	1.500	2.020	16.861	9.347	0.067	3.786	9.736

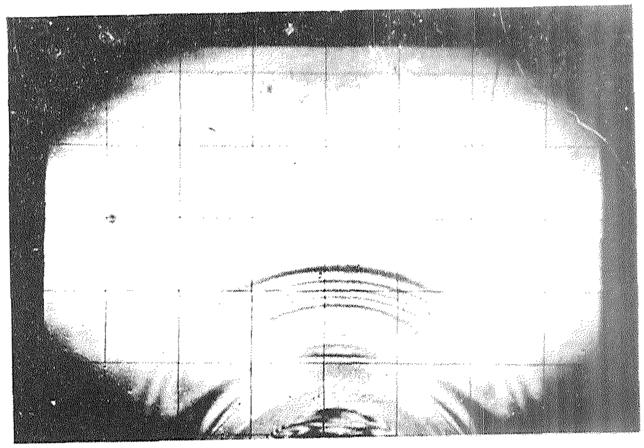

SHOT NUMBER 175, FRAME NUMBER [illegible]

	N	R	UR	ET	ER	SIGMA R	SIGMA THETA
1	0.0	3.450	0.0	0.0	0.0	[illegible]	[illegible]
2	0.500	3.360	0.124	0.037	[illegible]	[illegible]	[illegible]
3	1.500	3.210	0.933	[illegible]	[illegible]	[illegible]	[illegible]
4	2.500	3.080	2.713	0.731	[illegible]	[illegible]	[illegible]
5	3.500	2.950	4.346	1.408	[illegible]	[illegible]	[illegible]
6	4.500	2.840	6.920	[illegible]	[illegible]	[illegible]	[illegible]
7	5.500	2.700	10.013	[illegible]	[illegible]	[illegible]	[illegible]
8	5.500	2.640	[illegible]	[illegible]	[illegible]	[illegible]	[illegible]
9	4.500	2.580	[illegible]	[illegible]	[illegible]	[illegible]	[illegible]
10	3.500	2.470	[illegible]	[illegible]	[illegible]	[illegible]	[illegible]
11	2.500	2.390	[illegible]	[illegible]	[illegible]	[illegible]	[illegible]
12	1.500	2.300	15.503	[illegible]	[illegible]	[illegible]	[illegible]
13	0.800	2.210	[illegible]	[illegible]	[illegible]	[illegible]	[illegible]
14	1.000	2.150	[illegible]	[illegible]	[illegible]	[illegible]	[illegible]

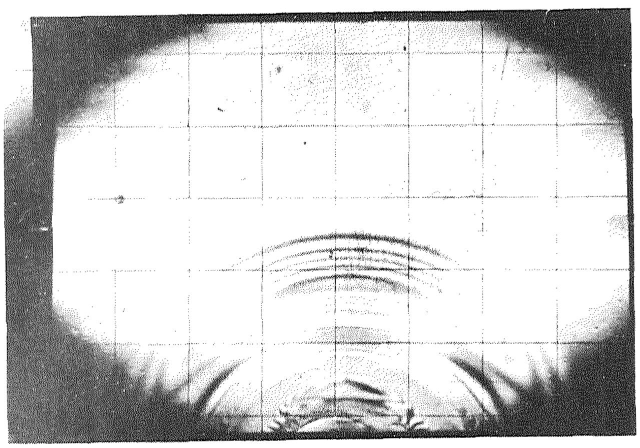

SHOT NUMBER 175, FRAME NUMBER 6

	N	R	UR	ET	ER	SIGMA R	SIGMA THETA
1	0.0	3.590	0.0	0.0	0.0	0.0	0.0
2	0.500	3.510	0.110	0.031	-2.729	-3.175	-1.175
3	1.500	3.360	0.925	0.275	-8.005	-9.233	-3.233
4	2.500	3.220	2.408	0.748	-13.052	-14.923	-4.923
5	3.500	3.090	4.427	1.433	-17.887	-20.270	-6.270
6	4.500	2.980	6.660	2.235	-22.605	-25.427	-7.427
7	4.500	2.790	11.133	3.990	-20.850	-22.596	-4.596
8	3.500	2.670	13.237	4.759	-14.361	-14.583	-0.583
9	2.500	2.570	14.365	5.589	-8.211	-7.115	2.885
10	1.500	2.470	14.882	6.025	-2.255	0.040	6.040
11	0.700	2.370	14.870	6.274	2.410	5.603	8.403
12	1.500	2.290	14.848	6.484	-1.796	0.780	6.780

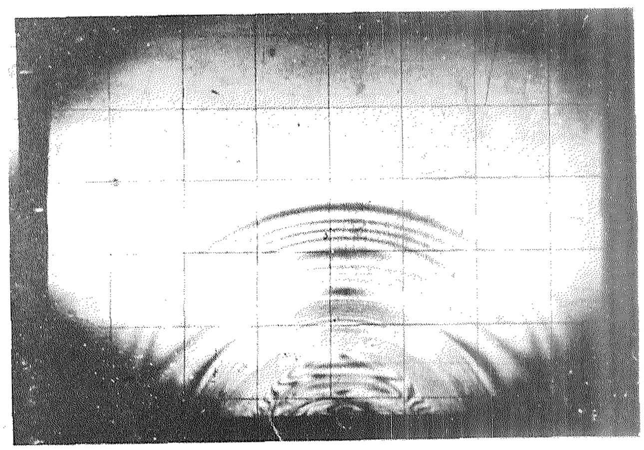

SHOT NUMBER 175, FRAME NUMBER [illegible]

	N	R	UR	ET	ER	SIGMA R	SIGMA THETA
1	0.0	3.750	0.0	0.0	0.0	0.0	0.0
2	0.500	3.670	0.110	0.030	-2.730	-3.177	-1.177
3	1.500	3.510	0.979	0.279	-8.001	-9.227	-3.227
4	2.500	3.373	2.463	0.731	-13.069	-14.950	-4.950
5	3.500	3.230	4.637	1.436	-17.884	-20.264	-6.264
6	4.500	3.093	7.470	2.418	-22.422	-25.133	-7.133
7	4.500	2.980	9.992	3.353	-21.487	-23.624	-5.624
8	3.500	2.840	12.532	4.413	-14.407	-15.463	-1.463
9	2.500	2.750	13.596	4.945	-8.855	-8.154	1.846
10	1.500	2.640	14.238	5.393	-2.887	-0.979	5.021
11	0.500	2.550	14.237	5.533	2.823	5.779	7.779
12	0.500	2.510	14.125	5.627	2.867	5.849	7.849

FIGURE 6

STRESS WAVE PHOTOGRAPHS AND COMPUTED RESULTS

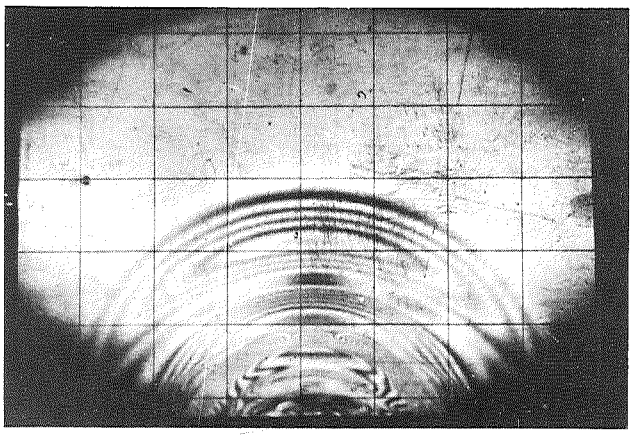

SHOT NUMBER 175, FRAME NUMBER 10

	N	R	DR	ET	ER	SIGMA R	SIGMA THETA
1	0.0	3.880	0.0	0.0	0.0	0.0	0.0
2	0.500	3.810	0.097	0.025	-2.735	-3.185	-1.185
3	1.500	3.660	0.913	0.249	-8.031	-9.275	-3.275
4	2.500	3.310	2.506	0.714	-13.086	-14.974	-4.974
5	3.500	3.360	4.836	1.440	-17.880	-20.258	-6.258
6	4.500	3.190	8.254	2.531	-22.249	-24.854	-6.854
7	4.500	3.150	9.164	2.789	-21.731	-24.340	-6.340
8	3.500	3.810	11.771	3.711	-15.409	-16.273	-2.273
9	2.500	2.920	12.883	4.412	-9.388	-9.013	0.987
10	1.500	2.810	13.344	4.834	-3.446	-1.880	4.120
11	0.500	2.700	13.642	5.052	2.292	4.923	6.923
12	0.350	2.670	13.566	5.079	3.147	5.933	7.333
13	0.500	2.650	13.503	5.056	2.336	4.994	6.994

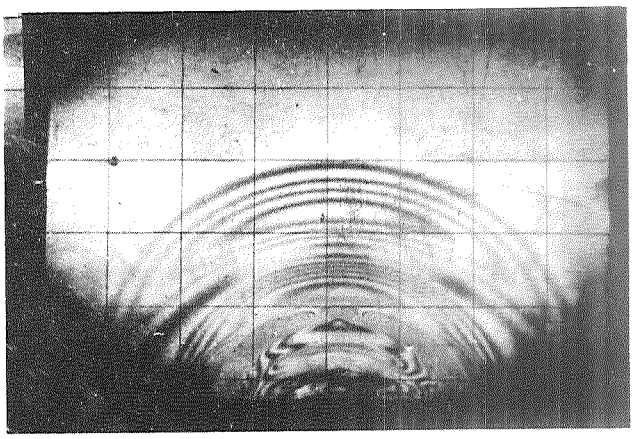

SHOT NUMBER 175, FRAME NUMBER 12

	N	R	DR	ET	ER	SIGMA R	SIGMA THETA
1	0.0	4.040	0.0	0.0	0.0	0.0	0.0
2	0.500	3.970	0.097	0.024	-2.736	-3.187	-1.187
3	1.500	3.810	0.967	0.254	-8.026	-9.268	-3.268
4	2.500	3.460	2.566	0.730	-13.100	-15.001	-5.001
5	3.500	3.500	5.096	1.444	-17.877	-20.253	-6.254
6	3.500	3.200	10.864	3.337	-15.923	-17.102	-3.102
7	2.500	3.090	12.280	3.774	-9.826	-9.711	0.281
8	1.500	2.580	13.036	4.573	-3.967	-2.625	1.375
9	0.500	2.875	13.140	4.578	1.818	4.159	6.159
10	0.200	2.830	13.035	4.605	3.501	6.137	6.938
11	0.500	2.780	12.839	4.640	1.980	4.253	6.253

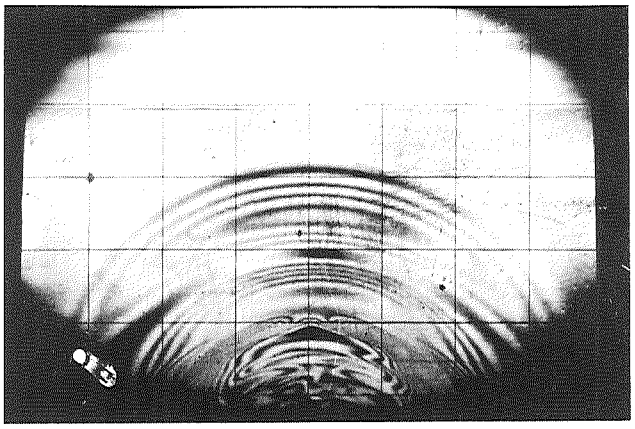

SHOT NUMBER 176, FRAME NUMBER 3

	N	R	DR	ET	ER	SIGMA R	SIGMA THETA
1	0.0	4.200	0.0	0.0	0.0	0.0	0.0
2	0.500	4.130	0.097	0.023	-2.737	-3.188	-1.188
3	1.500	3.970	0.966	0.244	-8.036	-9.284	-3.284
4	2.500	3.800	2.773	0.730	-13.070	-14.952	-4.952
5	3.500	3.640	5.259	1.445	-17.875	-20.250	-6.250
6	3.500	3.390	10.060	2.968	-16.352	-17.794	-3.794
7	2.500	3.280	11.521	3.513	-10.287	-10.464	-0.464
8	1.500	3.140	12.534	3.932	-4.288	-3.237	2.761
9	0.500	3.020	12.678	4.265	1.445	3.556	5.556
10	0.200	2.970	12.583	4.237	3.133	5.543	6.343
11	0.500	2.920	12.468	4.270	1.510	3.661	5.661

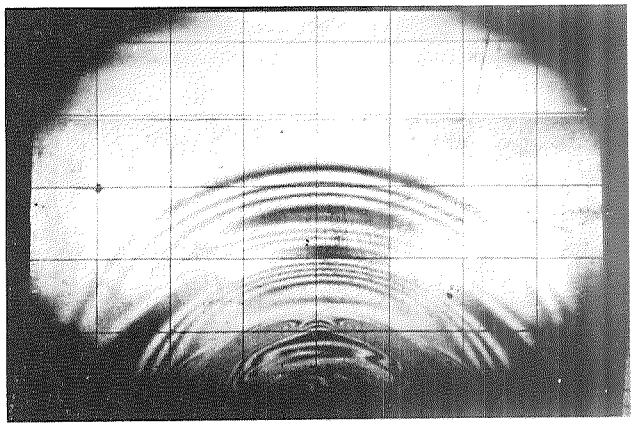

SHOT NUMBER 176, FRAME NUMBER 5

	N	R	DR	ET	ER	SIGMA R	SIGMA THETA
1	0.0	4.350	0.0	0.0	0.0	0.0	0.0
2	0.500	4.280	0.097	0.023	-2.737	-3.187	-1.187
3	1.500	4.120	0.968	0.235	-8.045	-9.298	-3.298
4	2.500	3.940	2.880	0.731	-13.064	-14.950	-4.950
5	3.500	3.770	5.521	1.464	-17.856	-20.219	-6.219
6	3.500	3.560	9.465	2.659	-16.661	-18.292	-4.292
7	2.500	3.420	11.356	3.321	-10.479	-10.773	-0.773
8	1.500	3.300	12.255	3.714	-4.566	-3.688	2.312
9	0.500	3.170	12.469	3.933	1.173	3.118	5.118
10	0.100	3.120	12.354	3.960	3.408	5.741	6.141
11	0.500	3.070	12.238	3.986	1.226	3.204	5.204

FIGURE 6 CONTINUED

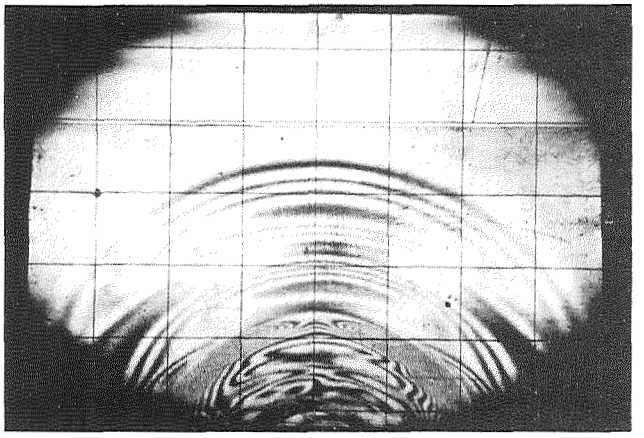

SHOT NUMBER 176, FRAME NUMBER 7

	N	R	UR	ET	ER	SIGMA R	SIGMA THETA
1	0.0	4.520	0.0	0.0	0.0	0.0	0.0
2	0.500	4.440	0.110	0.025	-2.735	-3.185	-1.186
3	1.500	4.260	1.089	0.256	-8.024	-9.265	-3.265
4	2.500	4.080	2.999	0.735	-13.065	-14.943	-4.943
5	3.500	3.910	5.640	1.443	-17.877	-20.254	-6.254
6	3.500	3.740	8.731	2.350	-16.970	-18.790	-4.790
7	2.500	3.610	10.594	2.935	-10.865	-11.396	-1.396
8	1.500	3.470	11.672	3.309	-4.911	-4.243	1.757
9	0.500	3.350	11.932	3.562	0.802	2.519	4.519
10	0.0	3.280	11.778	3.591	3.591	5.792	5.792
11	0.500	3.210	11.623	3.621	0.861	2.614	4.614

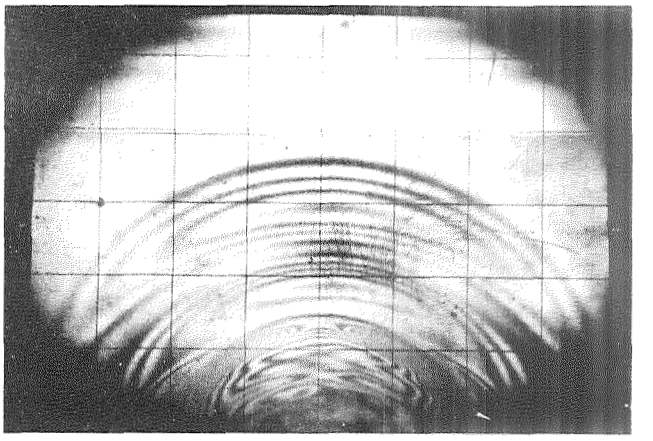

SHOT NUMBER 176, FRAME NUMBER 4

	N	R	UR	ET	ER	SIGMA R	SIGMA THETA
1	0.0	4.670	0.0	0.0	0.0	0.0	0.0
2	0.500	4.590	0.110	0.024	-2.736	-3.187	-1.187
3	1.500	4.420	1.036	0.234	-8.046	-9.287	-3.287
4	2.500	4.220	3.150	0.749	-13.051	-14.921	-4.921
5	3.500	4.050	5.830	1.432	-17.888	-20.271	-6.271
6	3.500	3.930	7.977	2.220	-17.299	-17.307	-5.307
7	2.500	3.770	10.239	2.716	-11.084	-11.748	-1.748
8	1.500	3.620	11.447	3.162	-5.118	-4.577	1.423
9	0.500	3.520	11.671	3.316	0.556	2.122	4.122
10	-0.050	3.430	11.491	3.341	3.623	5.721	5.561
11	0.500	3.350	11.313	3.377	0.617	2.221	4.221

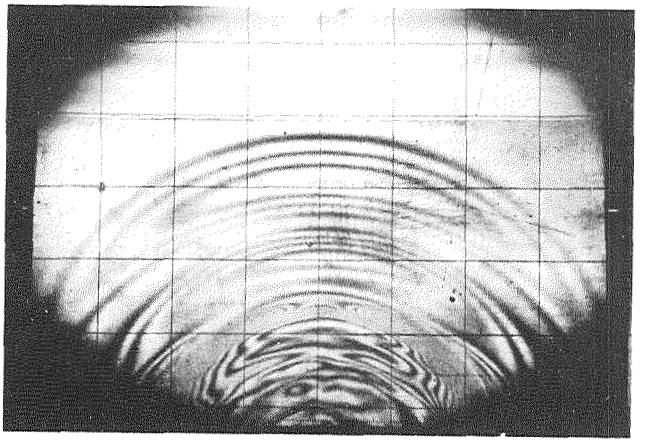

SHOT NUMBER 176, FRAME NUMBER 11

	N	R	UR	ET	ER	SIGMA R	SIGMA THETA
1	0.0	4.830	0.0	0.0	0.0	0.0	0.0
2	0.500	4.740	0.124	0.026	-2.734	-3.184	-1.184
3	1.500	4.560	1.104	0.242	-8.038	-9.287	-3.287
4	2.500	4.370	3.122	0.715	-13.085	-14.977	-4.977
5	3.500	4.190	5.924	1.414	-17.906	-20.300	-6.300
6	3.500	4.120	7.175	1.742	-17.578	-19.772	-5.772
7	2.500	3.950	9.627	2.437	-11.363	-12.198	-2.198
8	1.500	3.800	10.878	2.863	-5.417	-5.060	0.940
9	0.500	3.670	11.205	3.053	0.293	1.698	3.698
10	-0.100	3.570	11.006	3.083	3.635	5.618	5.218
11	0.500	3.470	10.809	3.115	0.355	1.798	3.798

FIGURE 6 CONCLUDED

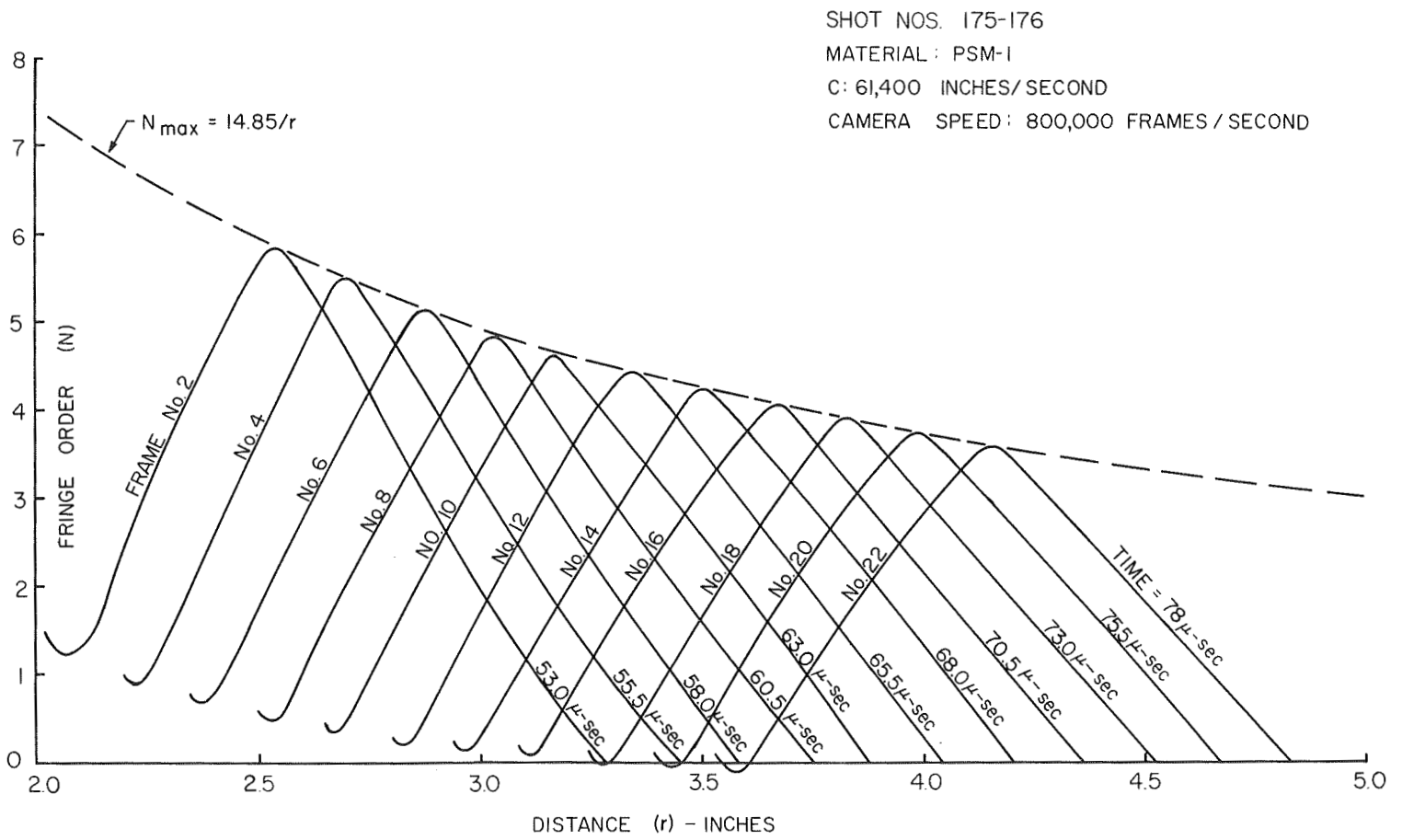

FIGURE 7

FRINGE NUMBER - DISTANCE - TIME RELATIONS

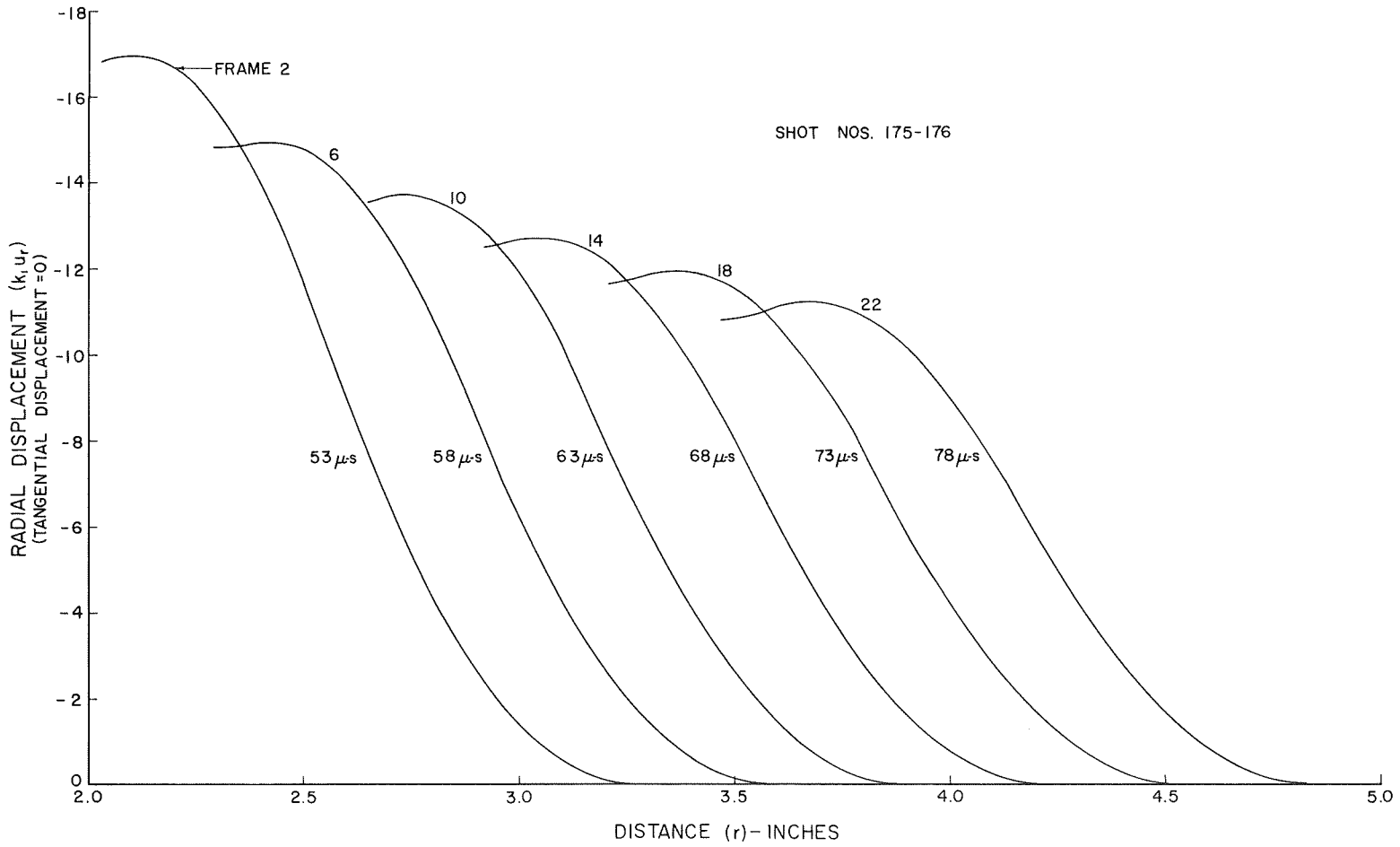

FIGURE 8

DISPLACEMENT - DISTANCE - TIME RELATIONS

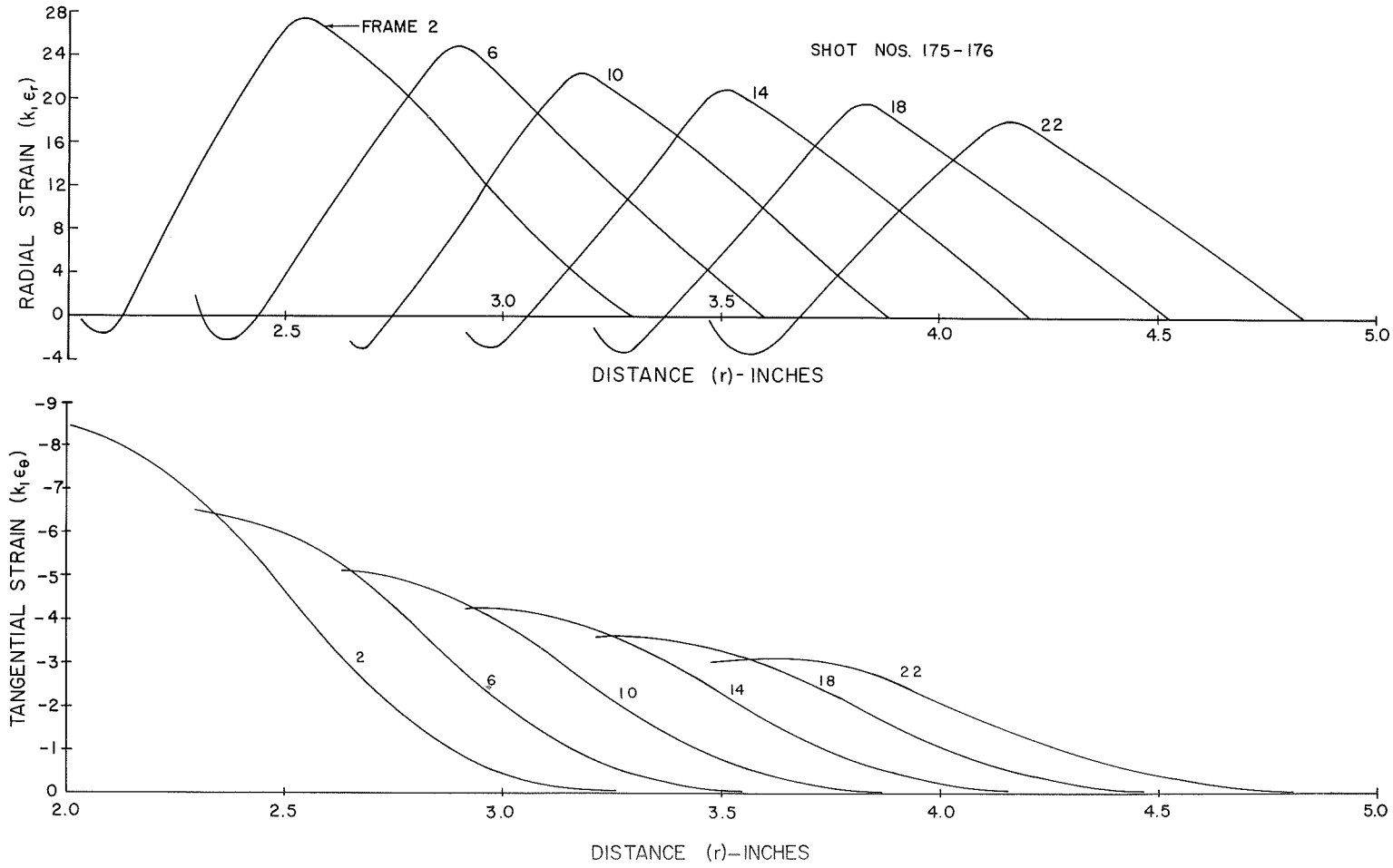

FIGURE 9

STRAIN-DISTANCE-TIME RELATIONS

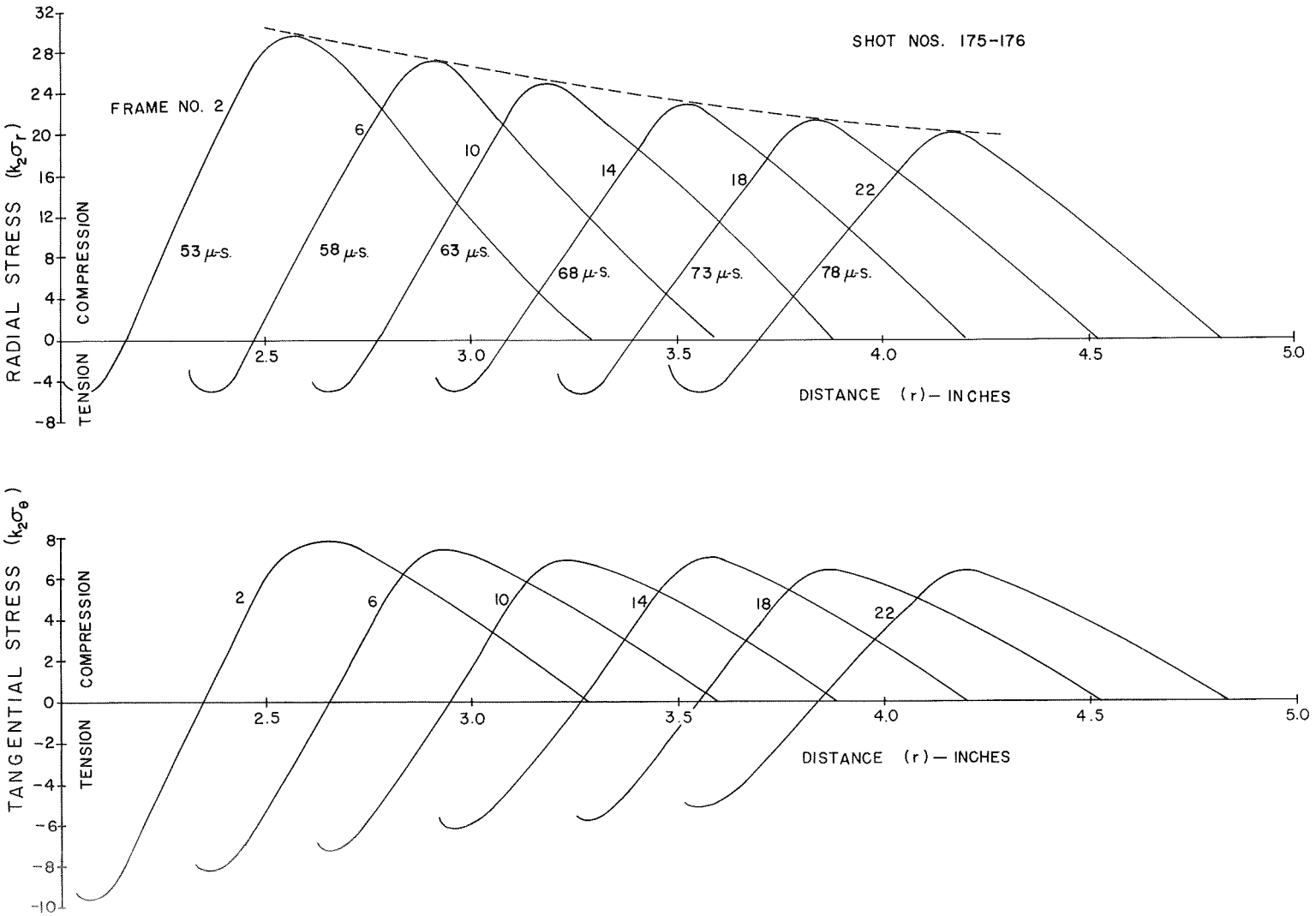

FIGURE 10

STRESS-DISTANCE-TIME RELATIONS

$\frac{1}{8}$" ALUMINUM LAMINATE (SHOT 240)

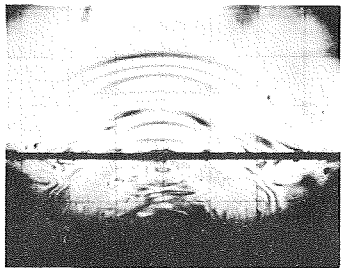

FRAME 1

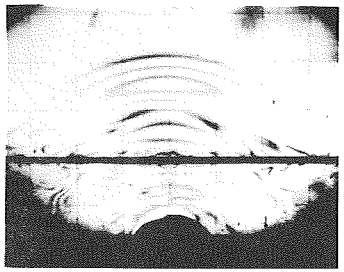

FRAME 2

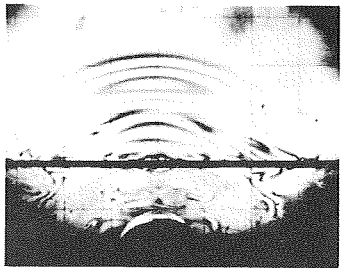

FRAME 3

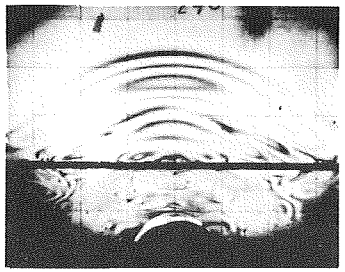

FRAME 4

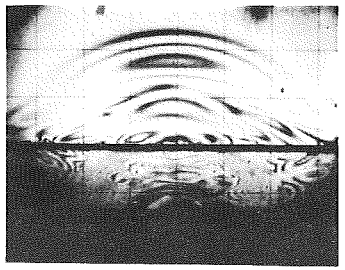

FRAME 5

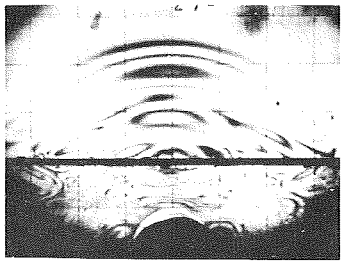

FRAME 6

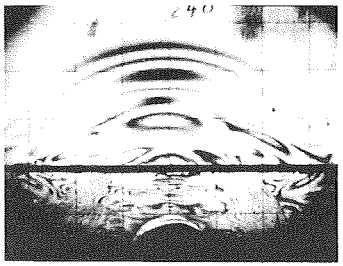

FRAME 7

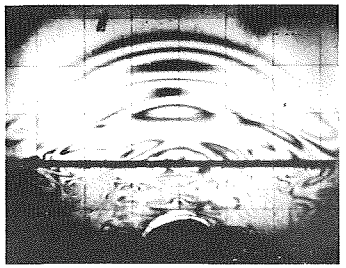

FRAME 8

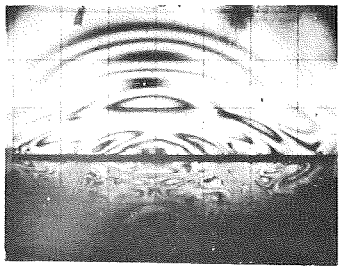

FRAME 9

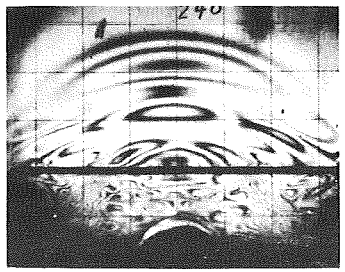

FRAME 10

FIGURE 11

STRESS WAVES THROUGH $\frac{1}{8}$ INCH ALUMINUM LAMINATE

1" ALUMINUM LAMINATE (SHOT 226)

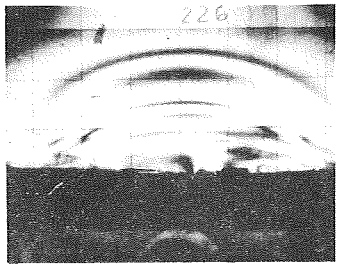

FRAME 1

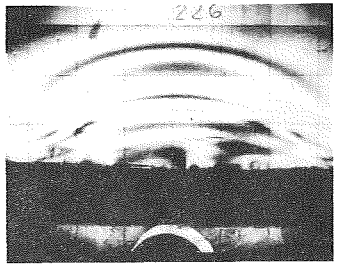

FRAME 2

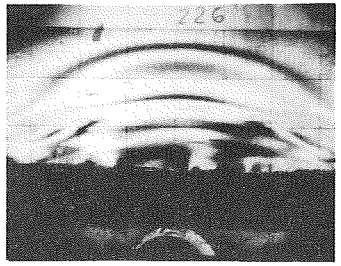

FRAME 3

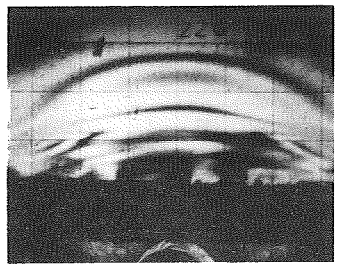

FRAME 4

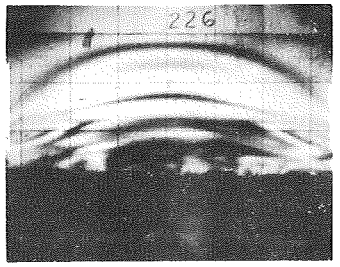

FRAME 5

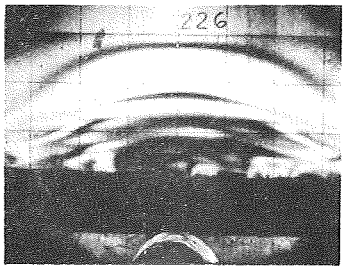

FRAME 6

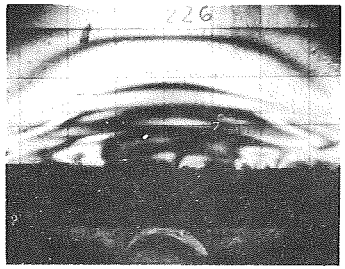

FRAME 7

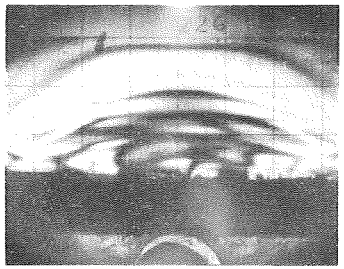

FRAME 8

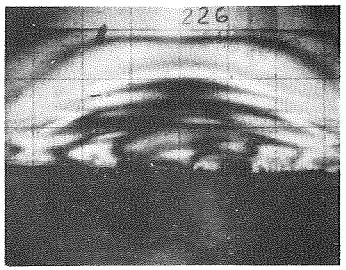

FRAME 9

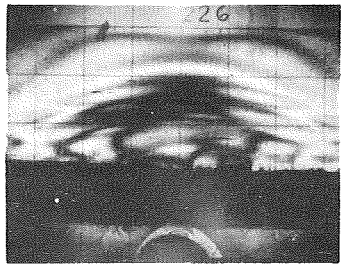

FRAME 10

FIGURE 12

STRESS WAVES THROUGH 1 INCH ALUMINUM LAMINATE

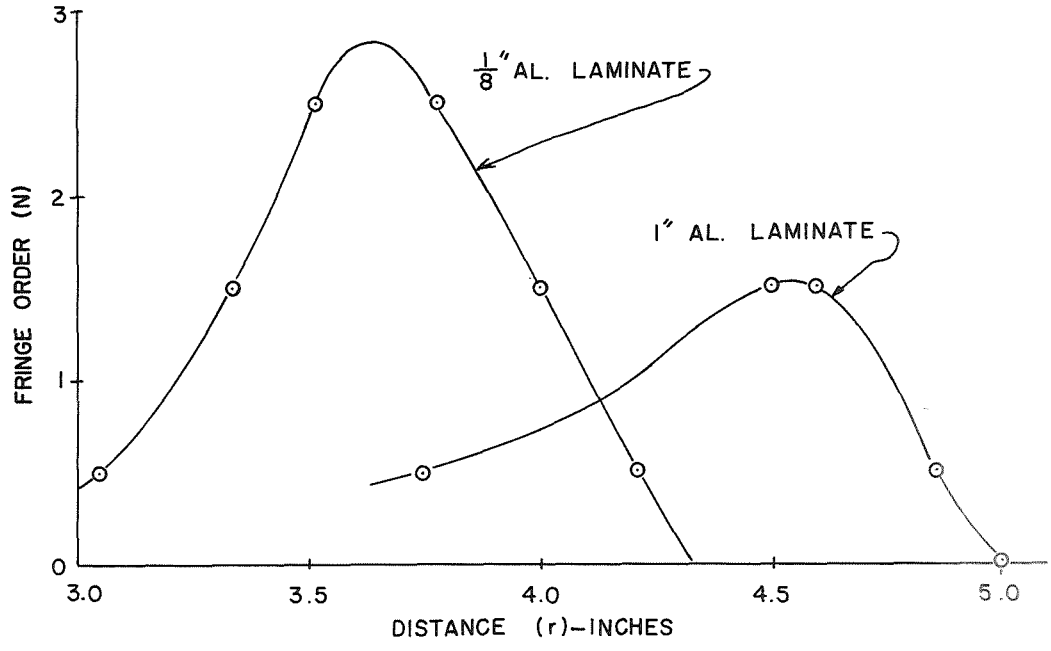

1/8 INCH LAMINATE							
	N	R	UR	ET	ER	SIGMA R	SIGMA THETA
1	C.C	4.330	0.0	0.C	0.C	C.C	0.0
2	C.500	4.210	0.166	0.039	-2.721	-3.162	-1.162
3	1.500	4.CCC	1.302	0.326	-7.954	-9.152	-3.152
4	2.500	3.780	3.609	0.955	-12.845	-14.589	-4.589
5	2.85C	3.7CC	4.7C2	1.271	-14.461	-16.337	-4.937
6	2.850	3.6CC	6.127	1.702	-14.030	-15.642	-4.242
7	2.500	3.510	7.285	2.076	-11.724	-12.781	-2.781
8	1.5CC	3.330	8.835	2.653	-5.627	-5.398	C.602
9	1.CCC	3.220	9.287	2.884	-2.636	-1.800	2.200
10	C.500	3.C5C	9.476	3.107	0.347	1.785	3.785

1 INCH LAMINATE							
	N	R	UR	ET	ER	SIGMA R	SIGMA THETA
1	C.C	5.CCC	C.C	0.C	0.C	0.C	0.C
2	C.500	4.86C	0.193	0.040	-2.720	-3.162	-1.162
3	1.CCC	4.760	0.600	0.126	-5.394	-6.248	-2.248
4	1.5CC	4.600	1.669	0.363	-7.917	-9.092	-3.092
5	1.5CC	4.5CC	2.452	0.545	-7.735	-8.799	-2.799
6	1.2CC	4.3CC	3.797	0.883	-5.741	-6.318	-1.518
7	1.CCC	4.2CC	4.308	1.026	-4.494	-4.797	-0.797
8	C.700	4.CCC	5.015	1.254	-2.610	-2.494	0.306
9	C.5CC	3.75C	5.499	1.466	-1.294	-0.861	1.139

FIGURE 13

FRINGE ORDER AND COMPUTED RESULTS - ALUMINUM LAMINATES

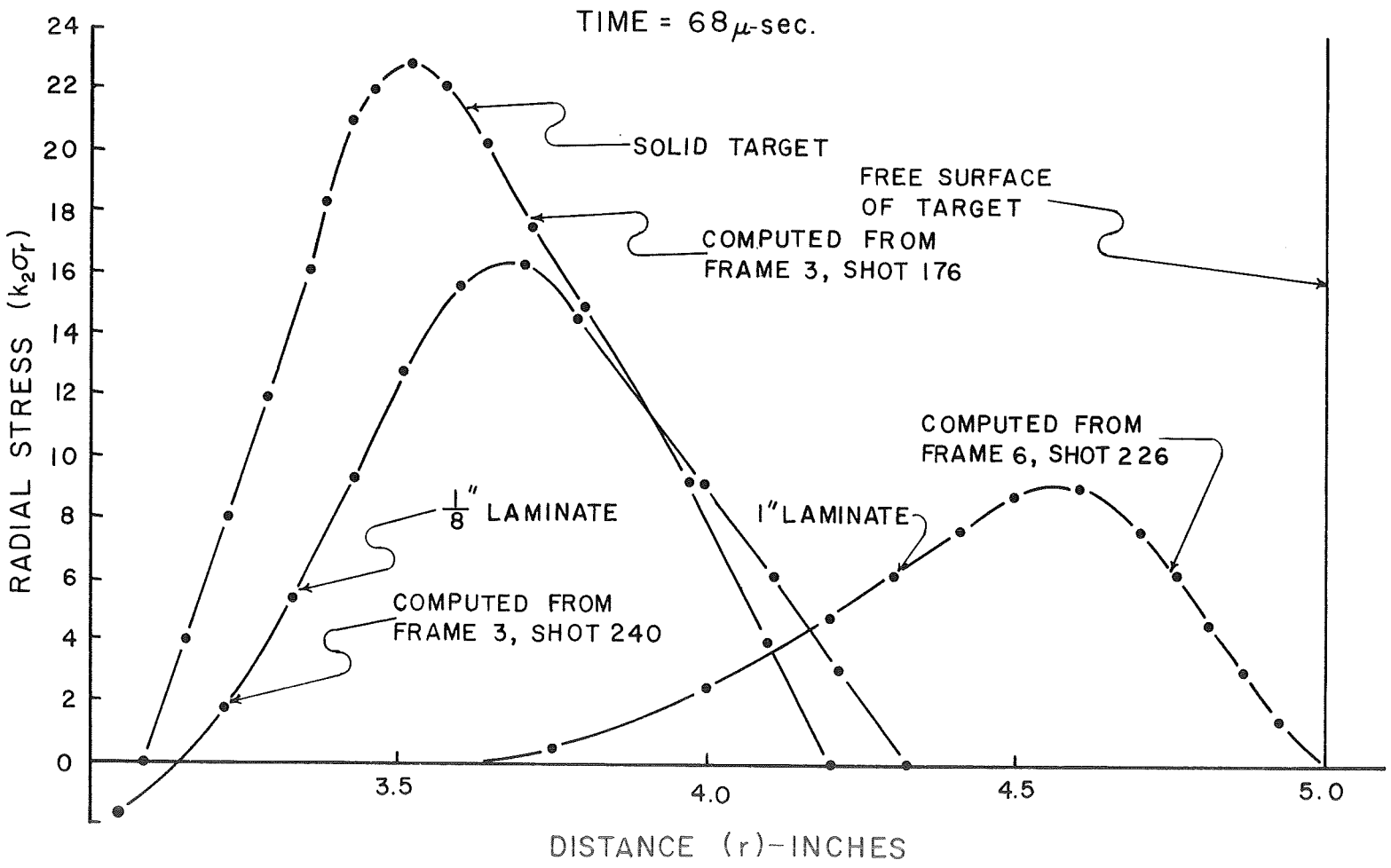

FIGURE 14

COMPARISON OF STRESSES IN HOMOGENEOUS AND LAMINATED TARGETS

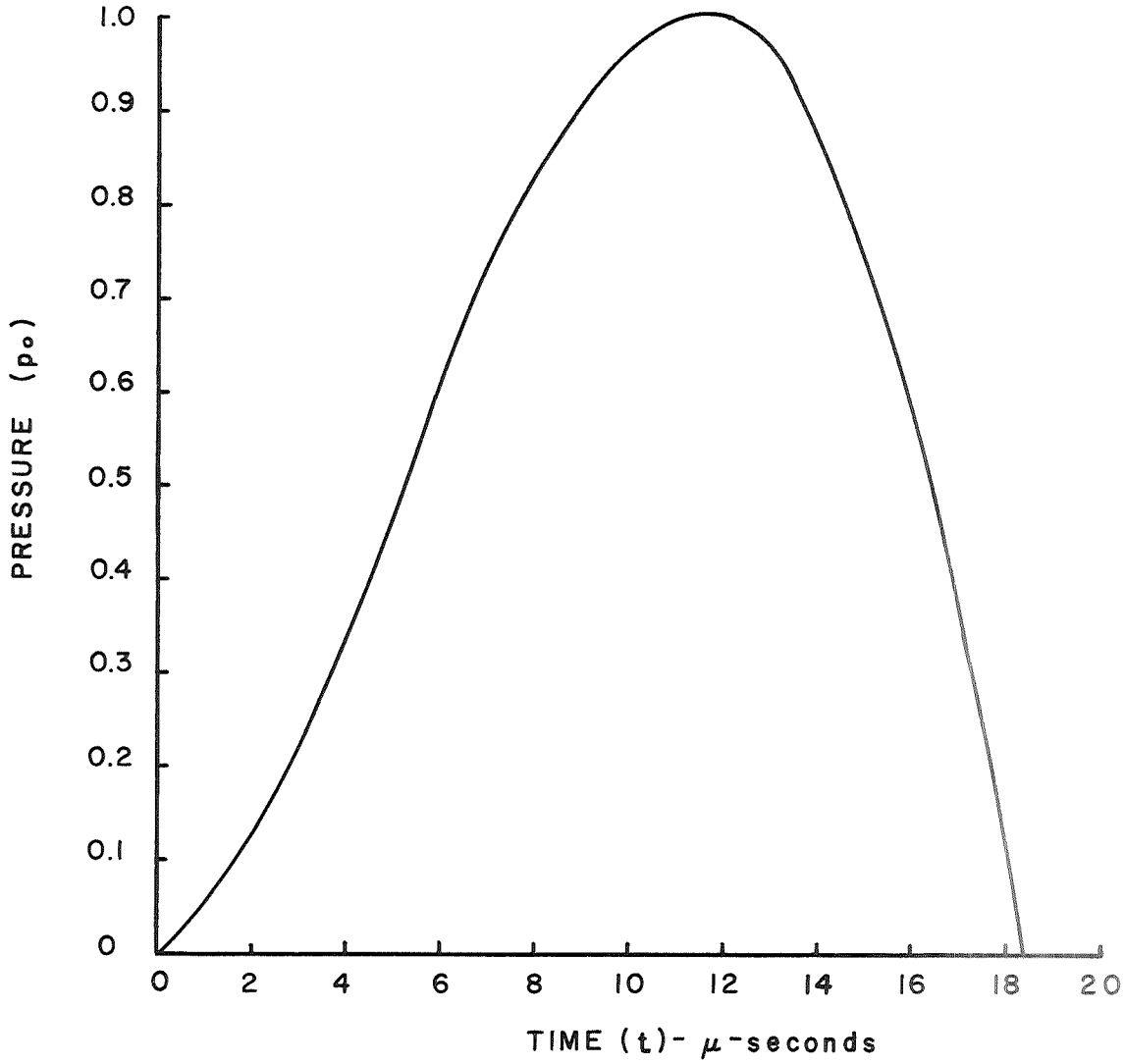

$$p_o = 9161\, e^{-0.01t} - 52194\, e^{-0.02t} + 116950\, e^{-0.03t} - 129079\, e^{-0.04t} + 70283\, e^{-0.05t} - 15121\, e^{-0.06t}$$

FIGURE 15

FORCING FUNCTION TO SIMULATE EXPERIMENTAL IMPULSE

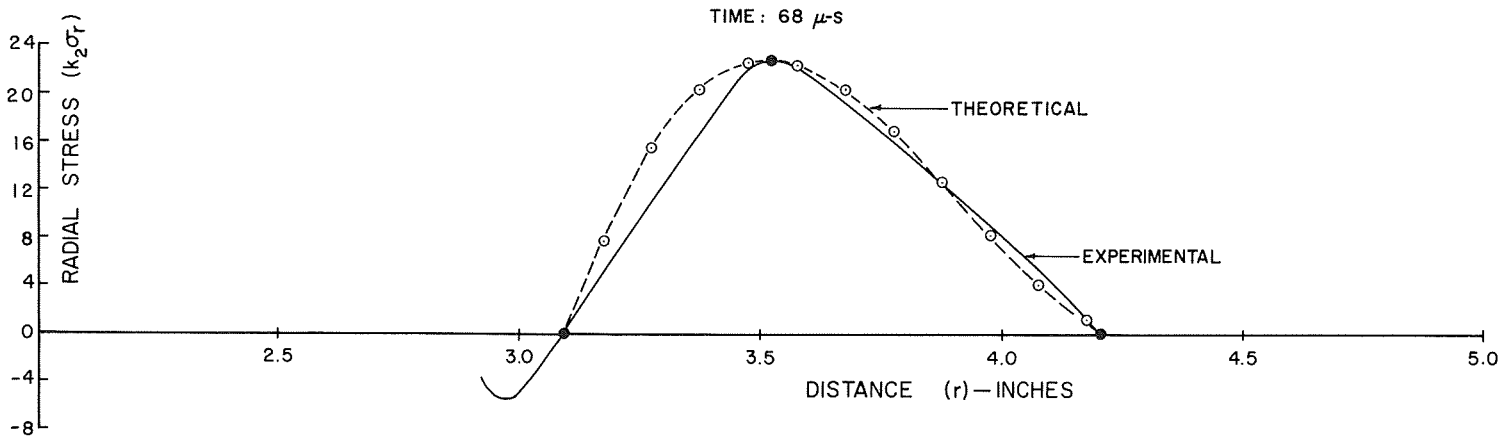

FIGURE 16

MATCHING THEORETICAL STRESS WAVE WITH EXPERIMENTAL STRESS WAVE

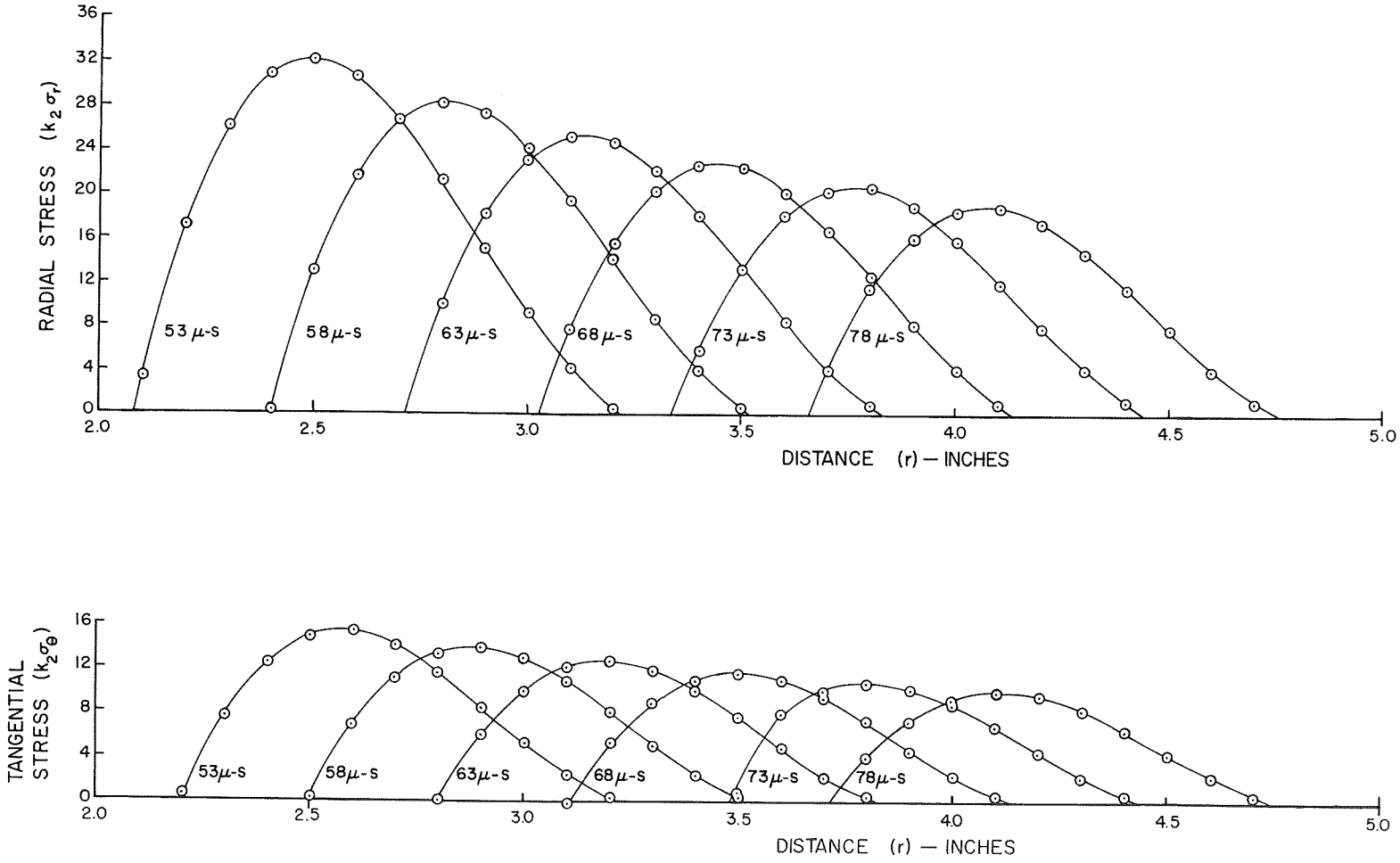

FIGURE 17

THEORETICAL STRESS-DISTANCE-TIME RELATIONS

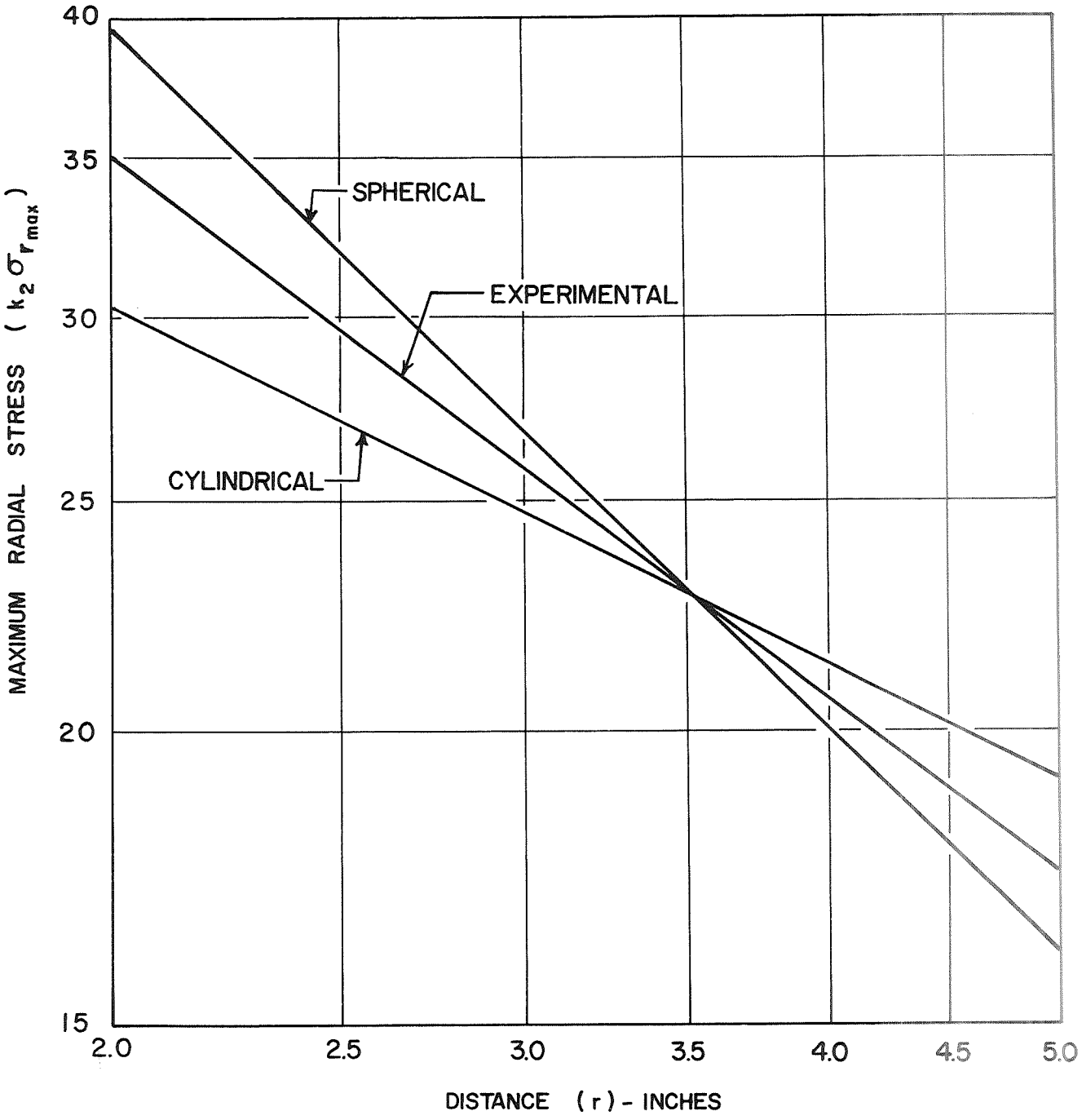

FIGURE 18

STRESS WAVE ATTENUATION

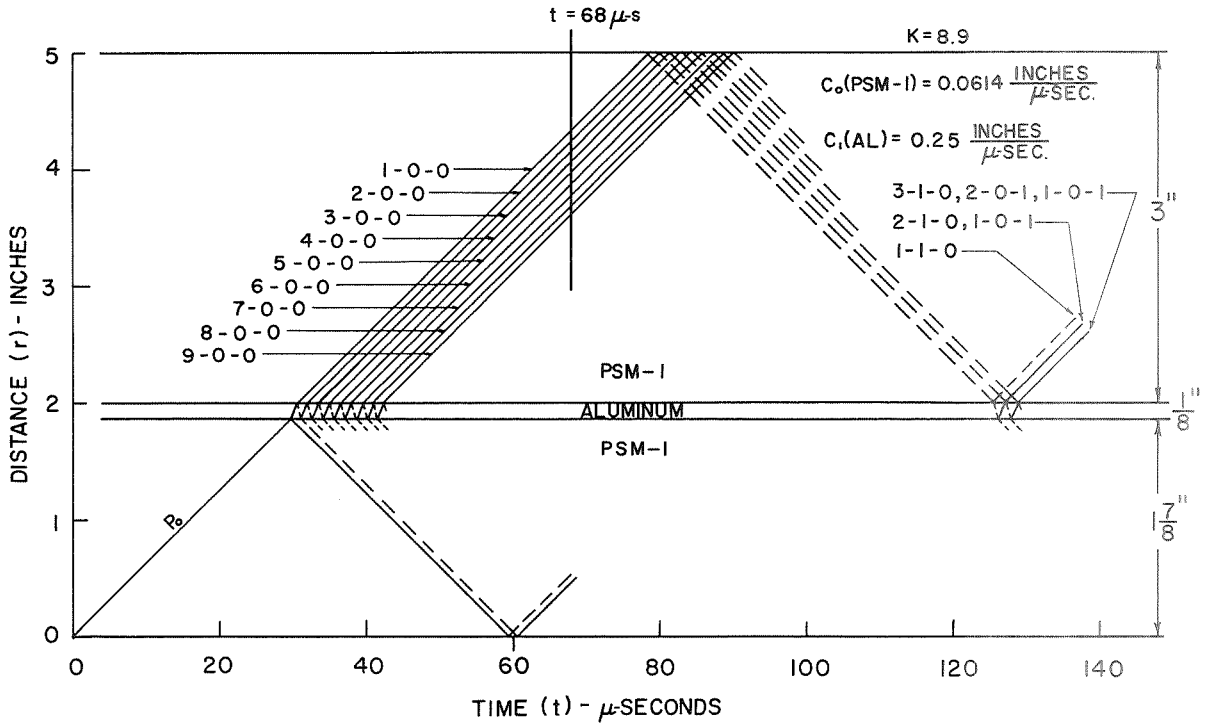

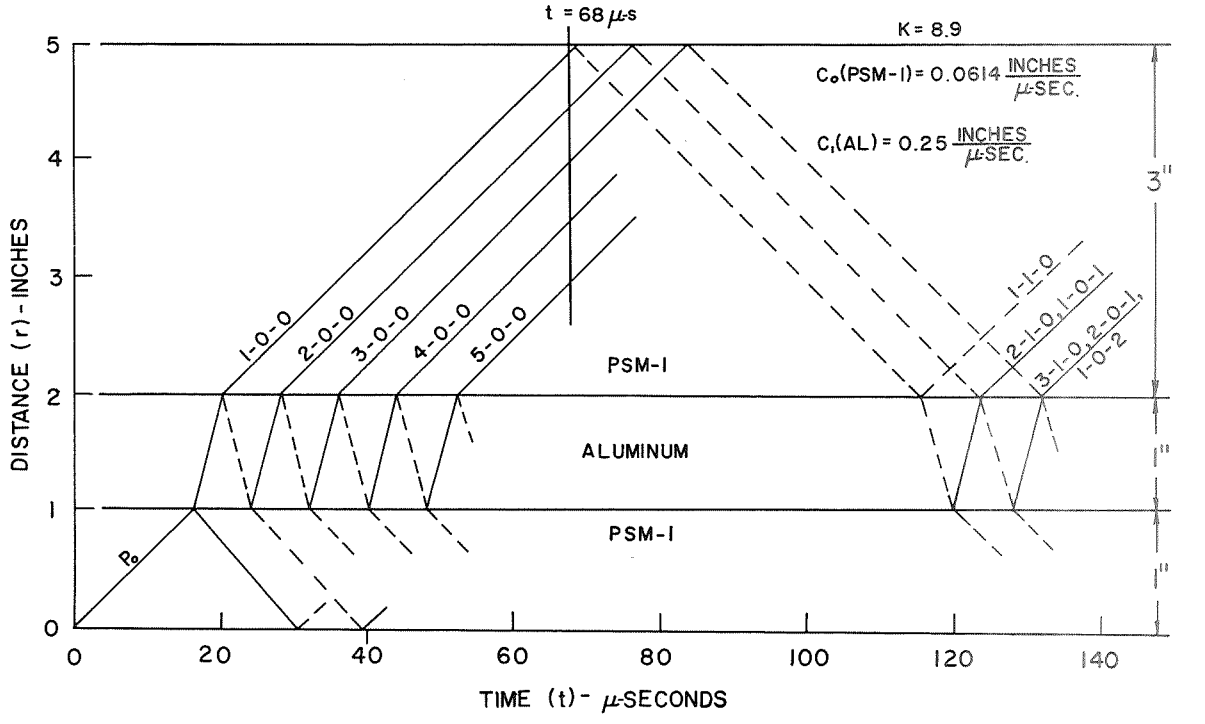

FIGURE 19

DISTANCE-TIME RELATION OF STRESS WAVES IN LAMINATED TARGETS

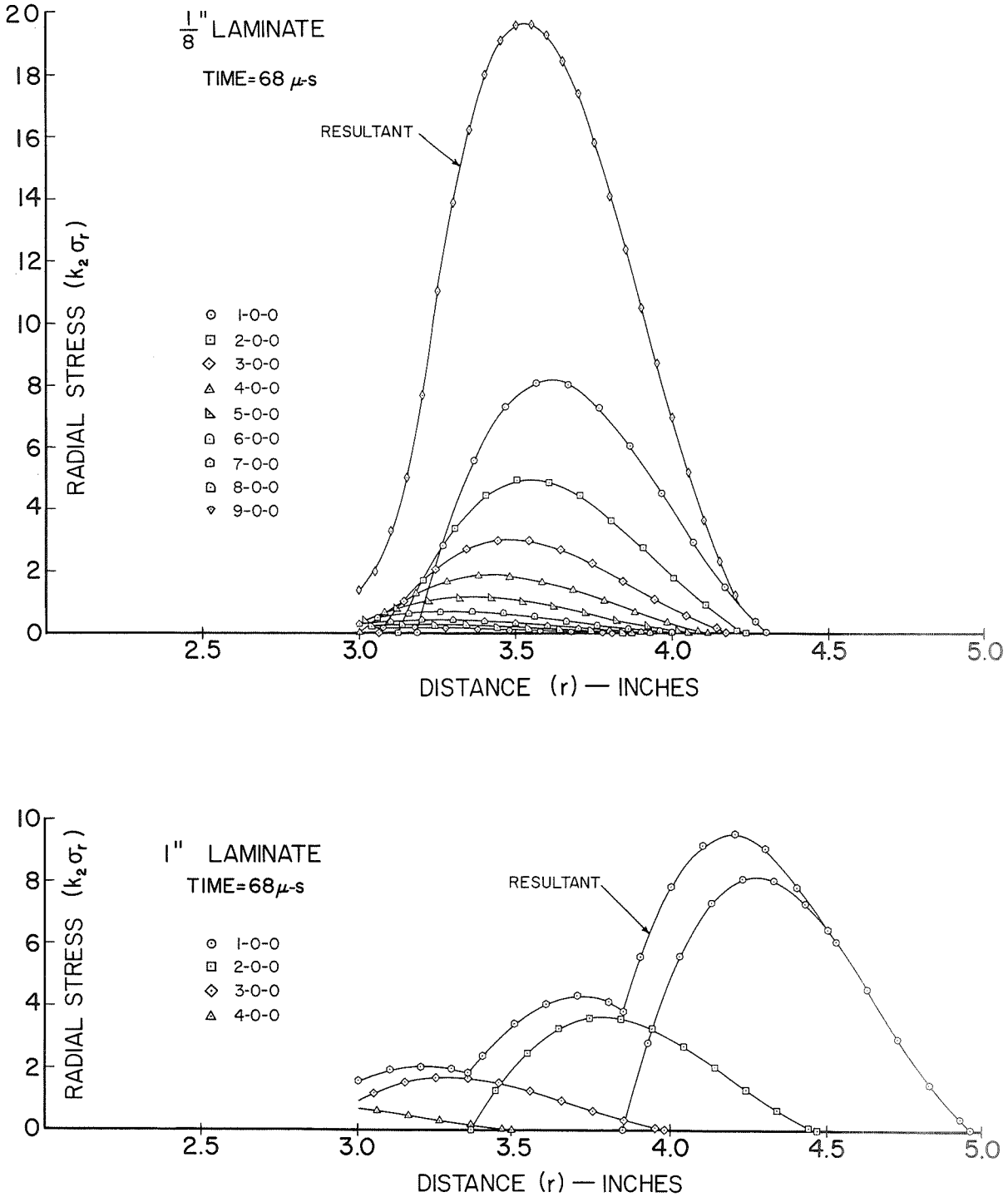

FIGURE 20

SUPERPOSITION OF TRANSMITTED STRESS WAVES IN LAMINATED TARGETS

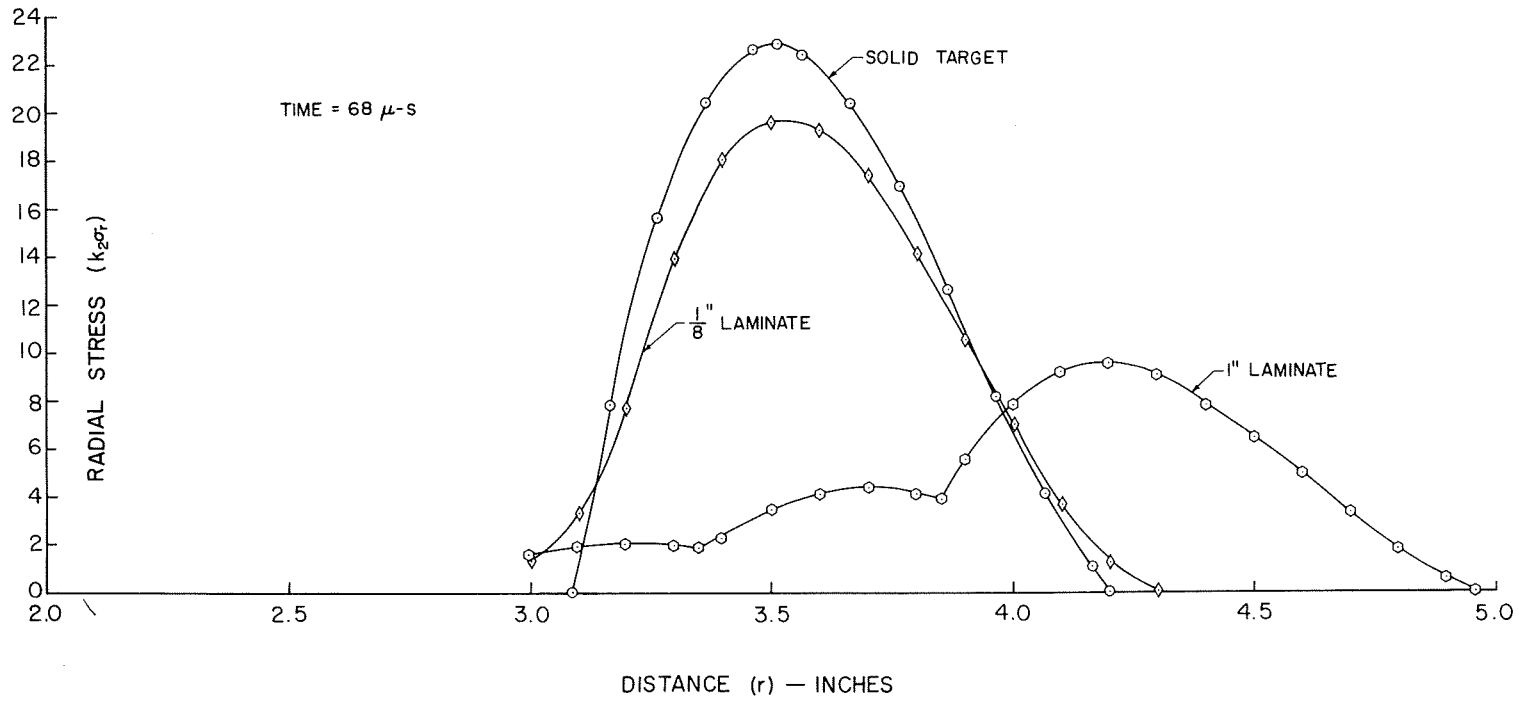

FIGURE 21

COMPARISON OF THEORETICAL STRESSES IN HOMOGENEOUS AND LAMINATED TARGETS

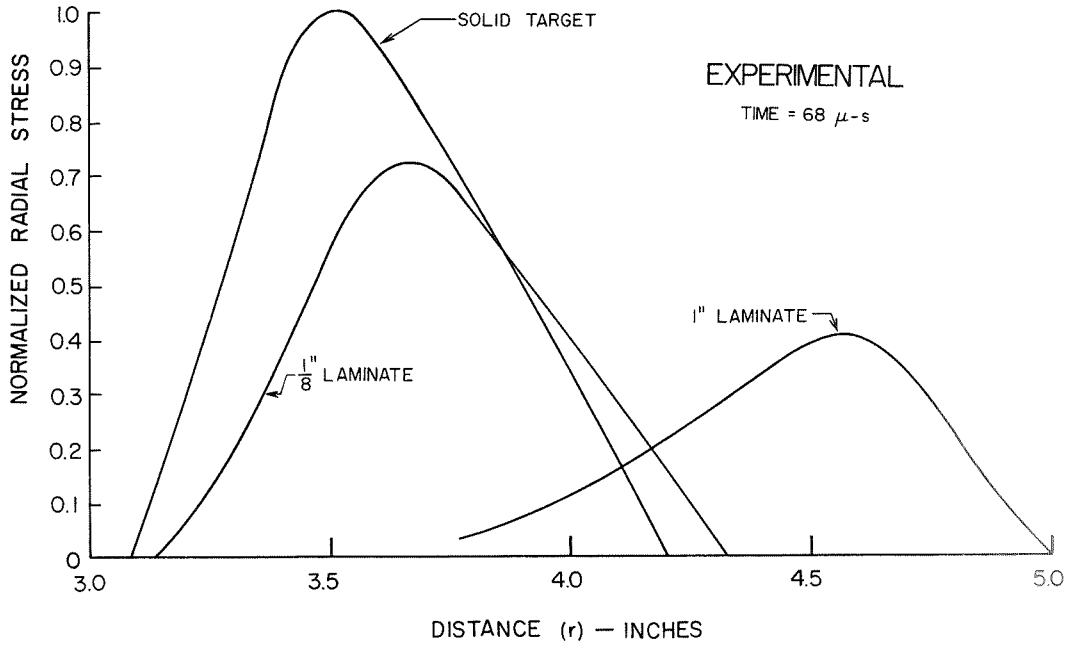

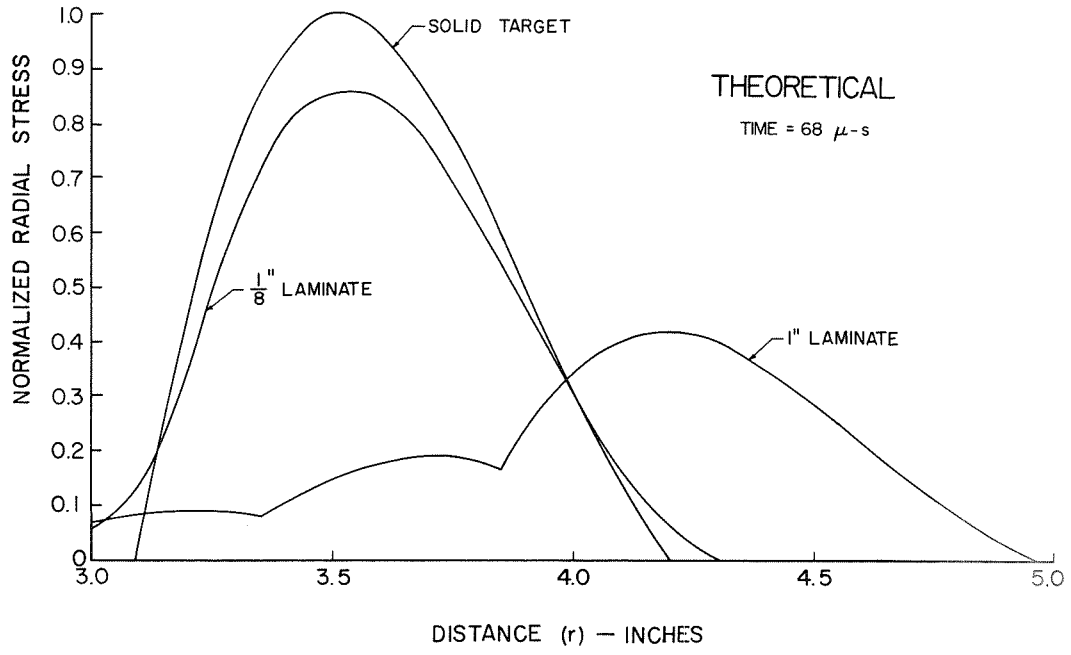

FIGURE 22

COMPARISON OF EXPERIMENTAL AND THEORETICAL RESULTS